Computational and Structural Biotechnology Journal 23 (2024) 2548–2564

Contents lists available at ScienceDirect

Computational and Structural Biotechnology Journal

journal homepage: www.elsevier.com/locate/csbj

# Mechanistic insights into P-glycoprotein ligand transport and inhibition revealed by enhanced molecular dynamics simulations

Ahmad Elbahnsi [a,*], Balint Dudas [a,1], Salvatore Cisternino [b], Xavier Declèves [b], Maria A. Miteva [a,*]

[a] Université Paris Cité, CNRS UMR 8038 CiTCoM, Inserm U1268 MCTR, Paris, France
[b] Université Paris Cité, Inserm UMRS 1144, Optimisation Thérapeutique en Neuropsychopharmacologie, Paris, France

ARTICLE INFO

*Keywords:*
ABC transporters
P-glycoprotein
ABCB1
Enhanced molecular dynamics
Translocation mechanisms

ABSTRACT

P-glycoprotein (P-gp) plays a crucial role in cellular detoxification and drug efflux processes, transitioning between inward-facing (IF) open, occluded, and outward-facing (OF) states to facilitate substrate transport. Its role is critical in cancer therapy, where P-gp contributes to the multidrug resistance phenotype. In our study, classical and enhanced molecular dynamics (MD) simulations were conducted to dissect the structural and functional features of the P-gp conformational states. Our advanced MD simulations, including kinetically excited targeted MD (ketMD) and adiabatic biasing MD (ABMD), provided deeper insights into state transition and translocation mechanisms. Our findings suggest that the unkinking of TM4 and TM10 helices is a prerequisite for correctly achieving the outward conformation. Simulations of the IF-occluded conformations, characterized by kinked TM4 and TM10 helices, consistently demonstrated altered communication between the transmembrane domains (TMDs) and nucleotide binding domain 2 (NBD2), suggesting the implication of this interface in inhibiting P-gp's efflux function. A particular emphasis was placed on the unstructured linker segment connecting the NBD1 to TMD2 and its role in the transporter's dynamics. With the linker present, we specifically noticed a potential entrance of cholesterol (CHOL) through the TM4-TM6 portal, shedding light on crucial residues involved in accommodating CHOL. We therefore suggest that this entry mechanism could be employed for some P-gp substrates or inhibitors. Our results provide critical data for understanding P-gp functioning and developing new P-gp inhibitors for establishing more effective strategies against multidrug resistance.

## 1. Introduction

The ABC transporters superfamily are highly prevalent membrane proteins distributed throughout various cellular tissues and serve essential physiological functions by facilitating the translocation of a wide array of compounds, both endogenous and exogenous. ABC transporters operate by harnessing the energy derived from the binding and hydrolysis of adenosine triphosphate (ATP) molecules, allowing them to transport these compounds against their concentration gradients [1–3]. Dysfunctions or excessive expression of ABC transporters have implications in various medical conditions. Their significance is emphasized by their role in conferring multidrug resistance (MDR) in cancer therapies, as well as their implication in the regulation of drug pharmacokinetics at critical physiological barriers, such as the blood-brain barrier, liver, kidney and intestine [4]. Additionally, the inhibition of ABC transporters, as well as drug-metabolizing enzymes, can result in drug-drug interactions (DDIs), which can influence the drug effectiveness and safety [4–6].

Human ABCB1, which is encoded by the ABCB1 gene and goes by the names P-glycoprotein (P-gp) or MultiDrug Resistance 1 (MDR1), belongs to the B-subfamily of ABC transporters. P-gp, known as the initial ABC efflux transporter identified in diverse drug-resistant tumors [7,8], demonstrates a codependent regulatory mechanism where the binding of a substrate influences ATPase activity, and conversely [9,10]. This intricate interplay between substrate binding and ATPase activity is a critical aspect of the transporter's function [10]. P-gp has a broad range of reported substrates and/or inhibitors, including various cytotoxic anticancer drugs, making it a central player in conferring resistance to a diverse array of pharmaceuticals [5,11]. Extensive research has been dedicated to understanding the protein's efflux function and developing

* Corresponding authors.
*E-mail addresses:* ahmad.elbahnsi@inserm.fr (A. Elbahnsi), maria.mitev@inserm.fr (M.A. Miteva).
[1] Current address: Department of Physics and Astronomy, University College London, London, UK

https://doi.org/10.1016/j.csbj.2024.06.010
Received 2 May 2024; Received in revised form 7 June 2024; Accepted 7 June 2024
Available online 13 June 2024

precise and effective P-gp inhibitors [12]. These inhibitors can be categorized into three generations. The first, like verapamil [13,14], showed significant toxicity at doses needed to reverse MDR [15]. Second-generation inhibitors, including dexverapamil [16], were more effective but metabolized by cytochrome P450 3A4, affecting their and co-administered drugs' profiles. Third-generation inhibitors [17,18], such as tariquidar, designed from structure-activity relationships, are effective at lower doses and not substrates of cytochrome P450 3A4, leading to fewer side effects. However, their failure in clinical trials highlights the challenge of drug behavior prediction in humans, underlining the need for better predictive models for clinical outcomes.

P-gp is composed of two transmembrane domains (TMDs) and two nucleotide-binding domains (NBDs). Each TMD contains six transmembrane helices: TM1 to TM6 form TMD1, while TM7 to TM12 form TMD2. These transmembrane helices are linked to each other by extracellular loops (ECLs) on the outer side and intracellular loops (ICLs) on the inner side of the plasma membrane. The two NBDs (NBD1 and NBD2) form two nucleotide binding sites (NBS) at the NBD1/NBD2 interface. These sites are crucial for ATP binding and hydrolysis, providing the energy required for the efflux pump function. Some NBS motifs are highly conserved within the ABC transporter superfamily, such as the ABC signature motif (LSGGQ), the Walker-A (incorporating a conserved K), Walker-B (with a conserved E), the H-loop and the Q-loop [19]. Additionally, a large, flexible, and unstructured linker spans between the C-terminal end of NBD1 and the N-terminal region of TMD2, a distinguishing segment particularly observed within the ABCB and C subfamilies. To facilitate its efflux pump function, P-gp undergoes dynamic transitions between an inward-facing (IF, open) state, facilitating the binding of compounds, and an outward-facing (OF, closed) state, enabling their expulsion at the extracellular space (see Fig. 1A). This dynamic structural alternation, which is characteristic of the alternating access mechanism, plays a crucial role in ensuring the efficient transport of ligands across the cell membrane, driven by the ATP-derived energy [9].

Three-dimensional structures of human P-gp have been experimentally determined using cryo electron microscopy (cryo-EM) in different conformational states (see the review [20]). These structures include ATP-free IF-occluded conformations [21–23], as well as an ATP-bound OF conformation [24]. In the IF-occluded states, P-gp exhibits kinked TM4 and TM10 helices, meaning these helices exhibit significant

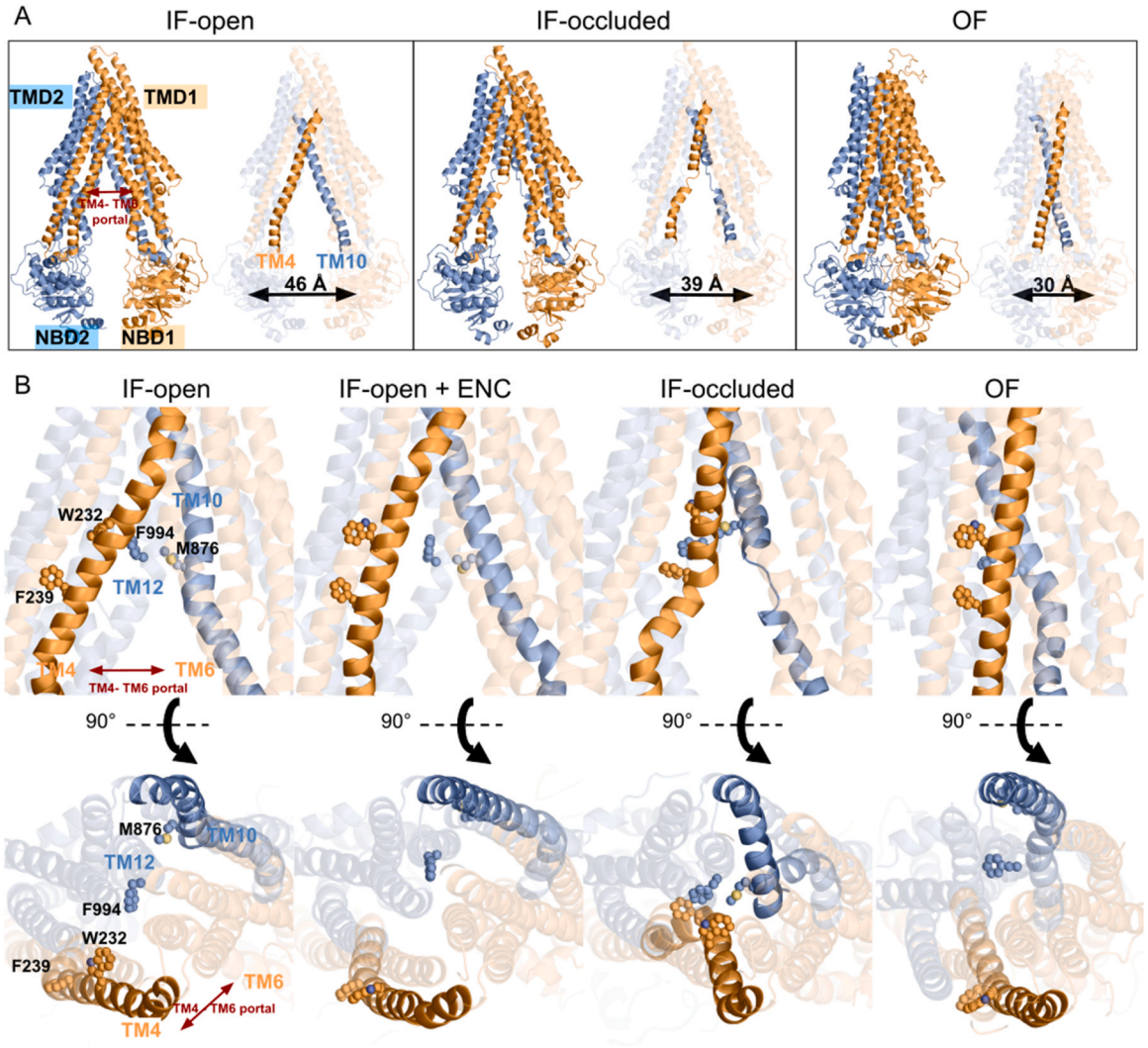


**Fig. 1.** Distinct conformations of P-gp. A) Initial models used for MD simulations, including the IF-open, IF-occluded and OF conformations. Each protein half is depicted in a distinct color: TMD1 +NBD1 in orange and TMD2 +NBD2 in blue. Conformations of TM4 and TM10 are highlighted. The TM4-TM6 portal is highlighted by a dark red double arrow on the IF-open conformation. B) Final snapshots from classical MD simulations of the IF-open, IF-open + ENC, IF-occluded and OF conformations, focusing on the TM regions, specifically on residues W232 and F239 in TM4, M876 in TM10, and F994 in TM12. These snapshots are presented from a side view (top) and a top/extracellular view (bottom). For enhanced clarity, all helices, except for TM4 and TM10, are rendered as transparent. The TM4-TM6 portal is highlighted by a dark red double arrow on the IF-open conformation.

break/bend, which result in closer NBDs compared to the wide IF-open conformation observed in mouse P-gp, characterized by canonical straight TM4 and TM10 helices [25,26]. In fact, the IF-occluded conformations were captured in the presence of the Fab fragment of an inhibitory monoclonal antibody, MRK16 or UIC2, which may be responsible for stabilizing the IF-occluded conformation [21]. Furthermore, the IF-occluded structures were determined in the presence of various substrates, including antitumor compounds such as taxol and vincristine, as well as third-generation inhibitors like tariquidar, elacridar, zosuquidar, as well as encequidar [21–23].

These structural data have yielded valuable insights into the binding cavity of P-gp, which can be divided into three distinct regions, as proposed by the Locher group [21], comprising a central drug binding pocket, an access tunnel accessible starting at the TM4/TM10 gate, and a vestibule where the access tunnel connects with the central drug-binding pocket. Notably, P-gp structures with substrates contain only one molecule within the central drug-binding pocket. In contrast, when inhibitors are present, two molecules, adopting U- and L-shaped conformations, are found one above the other within the transporter cavity. Substrates and U-shaped inhibitors are both situated in the central drug-binding pocket, while the second L-shaped inhibitors extend from the vestibule to the access tunnel [21]. Nonetheless, previous experimental studies suggested the existence of multiple distinct drug-binding sites, including at least four distinct sites classified as transport or regulation sites [27,28].

In addition, in the available experimental 3D structures, the linker segment remains unresolved, likely due to its considerable flexibility stemming from a lack of stable secondary structures. Such region, encompassing around 70 amino acids in P-gp, is typically found in the transporters from the ABCB subfamily [9] and the ABCC family (e.g. the CFTR anion channel [29,30]). In P-gp, the linker is believed to play a significant role in substrate poly-specificity and in controlling the flexibility and transport cycle of P-gp [20]. Multiple studies have provided evidence that phosphorylation of the linker in human P-gp is the means by which this regulation is achieved [31]. Indeed, dephosphorylation of the typically phosphorylated linker reduces substrate-induced ATPase activity [32]. Moreover, shortening of the linker has been found to abolish substrate stimulation of ATPase activity and significantly reduce transport [33].

Despite the substantial knowledge available about P-gp, several critical questions remain unanswered. The existing cryo-EM structures offer static snapshots but fail to elucidate the complete substrate translocation/ATP hydrolysis cycle of the transporter. While numerous studies provided valuable insights into transported or inhibiting compounds and their interactions, they do not provide a clear understanding of the molecular mechanisms governing substrate recognition promiscuity, the efflux pathway process, or the interplay between substrate binding/transport and ATP binding/hydrolysis. Furthermore, although the IF-open and OF conformations have received extensive attention, there is a notable lack of studies concerning the recent cryo-EM solved IF-occluded conformations, which may hold the key to predicting more effective P-gp inhibitors.

In this study, we employed both conventional and enhanced molecular dynamics (MD) simulations to conduct an in-depth analysis of the three distinct key states (IF-open, OF and IF-occluded) of P-gp, in the absence or presence of a substrate or an inhibitor. Our findings elucidate the mechanisms of conformational transitions between these states, highlight the protein's plasticity to accommodate various ligands through a primary lateral portal in the transmembrane region, and yield new insights into the substrate translocation pathways. Additionally, we highlight the crucial role of the linker domain in stabilizing the different conformational states. Our analyses also suggest a potential inhibition mechanism involving allosteric modulation through a TMD-NBD2 interface. Finally, our simulations offered additional transient conformations, opening the door for the development of structure-based predictive models of P-gp substrates and inhibitors.

## 2. Materials and methods

### 2.1. Models of P-gp, substrate and inhibitor compounds

Human P-gp cryo-EM structures for the OF (PDB code: 6C0V [24]) and for the IF-occluded (PDB code: 7O9W[22]) conformations, as well as the Alphafold2 model for the IF-open conformation, were used as initial states for standard MD simulations and as targets for the ketMD/ABMD simulations (see below). In all systems, the N-terminal (aa 1–35) and C-terminal (aa 1276–1280) segments were discarded while models with and without the linker (aa 630–695) were considered. The ECL1 loop was absent in the cryo-EM structures and was subsequently constructed using the Modeller [34,35]. Models including the linker were provided by Alphafold2 [36,37] (from AlphaFold Protein Structure Database: https://alphafold.ebi.ac.uk/) for the IF-open conformation and by iTasser [38,39] for the OF and IF-occluded systems. AlphaFold2, known for its high-confidence predictions generated through deep learning, provided confident models of the IF-open state, likely due to the abundance of inward-facing open ABC transporter 3D structures in the PDB. However, it struggles with different conformational states, leading to our unsuccessful attempts to generate OF and IF-occluded states. Therefore, we used iTasser to produce models for the OF and IF-occluded conformations, using the cryo-EM structures 6C0V and 7O9W as structural templates, respectively. For these states, our primary focus was on modeling the linker region, as the rest of the protein (the TMDs and NBDs) were already obtained experimentally by cryo-EM. Five linker models were generated per state, and selection for MD was based on visual inspection, discarding those with steric clashes or inconsistent linker paths (e.g. passage between ICL domains). This approach allowed us to maintain the experimentally observed conformations of the TMDs and NBDs while generating different conformations of the linker region.

We selected as a substrate vincristine (VIN) (Fig. S1), a chemotherapy drug used to treat various types of cancer, which is found bound to an IF-occluded P-gp in a cryo-EM structure (PDB 7A69). IF-open systems with VIN were built by carrying out a structural alignment of the Alphafold model with the protein in 7A69 [21] from which the substrate was extracted. Encequidar (ENC) (Fig. S1), an analog of tariquidar, a third-generation P-gp inhibitor, was chosen as it was already within the IF-occluded cryo-EM structure used for the protein model (PDB 7O9W[22]). While there were two molecules located in two different sites within the TMDs, one above the other, we chose to keep only the lower and more extended molecule suggesting more structural impact on the transport/inhibitory mechanisms. The topology and parameter files, used for subsequent molecular dynamics simulations (see next section), for VIN and ENC were generated using the CgenFF module in charmm-gui server [40–43]. The protonation state was determined for both ligands at pH 7.4 by the CgenFF module and by using the major macrospecies option of the ChemAxon calculator plugins (www.chemaxon.com) resulting in two positively charged nitrogens in VIN (on N4 and N1 atoms) and one in ENC (on N1 atom).

### 2.2. Molecular Dynamics (MD) simulations

Each system was prepared with the charmm-gui server [40–43]. Missing atoms were added. Patches were applied at both the N-terminal and C-terminal ends on each half transporter. Each model was then embedded in a lipid bilayer composed of cholesterol (outer leaflet: 20 % / inner leaflet: 20 %), POPC (1-palmitoyl-2-oleoyl-sn-glycero-3-phosphocholine) (60 % / 60 %), POPS (1-palmitoyl-2-oleoyl-sn--glycero-3- phospho-L-serine) (0 % / 20 %) and sphingolipids (DSM) (20 % / 0 %). The proportions of lipids reflect the composition of lipids in blood epithelial cells membrane according to [44]. The orientation and spatial positioning (insertion depth) of the protein within the lipid bilayer was estimated using the PPM (Positioning of Proteins in Membranes) server [45,46].

The protein, lipids, ATP and ions were modeled using the

CHARMM36m force field [47,48], and the TIP3P model was employed for water. The Force field parameters for VIN and ENC were built with charmm-gui with the Ligand Modeler module generating topology and parameter files of the ligands using CgenFF [40–43]. The calculations involved a series of steps, including minimization, equilibration, and production runs, which were executed using different versions of Gromacs [49,50] (2019.3, 2020.3, 2021.7 and 2023), depending on the specific computer, server and computational center employed. During minimization and equilibration steps, the default CHARMM-GUI inputs were used. Harmonic restraints were initially placed on the heavy atoms of the protein and the lipids, with a gradual release over a period of 1.875 ns.

The production dynamics was conducted in the NPT ensemble, without any restraints, and temperature and pressure were maintained at 310 K and 1 bar, respectively, using the Nose–Hoover thermostat [51] and Parrinello–Rahman barostat [52]. Periodic boundary conditions were applied, and long-range electrostatic interactions were treated using the particle mesh Ewald algorithm [53], with a switching function employed between 10 and 12 Å for non-bonded interactions. Bond lengths involving hydrogen atoms were constrained using LINCS [54]. The integration timestep was set at 2 fs, and the total trajectory length ranged from 100 to 300 ns.

### 2.3. Kinetically excited targeted MD (ketMD)

We recently developed an original enhanced sampling method for molecular dynamics (MD), namely kinetically excited targeted MD, that allowed us to reveal the transitions between the inward and outward-facing states and the ligand translocation pathway in BCRP (ABCG2), another important ABC transporter involved in MDR [55].

In the same way, we adapted ketMD to model transitions between distinct states and investigate the transportation of VIN, a substrate of P-gp. As detailed in [55], ketMD is based on kinetic excitations. In each excitation cycle, the velocity components pointing from the instantaneous conformation to the target are increased at the first step of the MD simulation. Then, the injected kinetic energy dissipates during a relaxation period while no external perturbation is introduced, and the system progresses.

The kinetic excitation corresponded to an overall temperature rise of 2 or 4 K across the systems. As the excitation kinetic energy dissipates rapidly (in less than 1 ps), 40 or 50 consecutive excitation cycles were performed, each containing a 6 ps relaxation MD simulation. Thus, the total ketMD simulation time was either 240 ps (for 40 cycles) or 300 ps (for 50 cycles), depending on the system in question. We performed ketMD simulations with excitation applied also to the substrate, starting from the IF-open-VIN model. The velocity components of the substrate, perpendicular to the membrane surface pointing to the extracellular space, were also increased at the first step of the MD simulations in each excitation cycle, corresponding to an additional 0.5 K temperature rise of the given system.

### 2.4. Adiabatic Bias MD (ABMD)

ABMD simulations were carried out using gromacs 2019.6 and the same simulation conditions described above [56]. In this method, a ratchet-like biasing harmonic potential is added, encouraging further exploration of the Collective Variable (CV) space. In these simulations, Plumed 2.8.2 [57] was called along the MD production during 10 ns to apply a bias on a selection of CVs, namely the distance between the center of mass of pairs of residues or segments. The bias was applied based on target distances that served as a threshold, where the bias between pairs was turned off if the distance evolved below or above the target values. A distance target T0 and a bias force constant KAPPA between 3000.0 and 10000 kJ/mol were set for each CV.

### 2.5. Analysis tools

Root Mean Square Deviation (RMSD) calculations for the protein were conducted using a Tcl VMD script and plotted using R. These calculations were performed on the Calpha atoms of the transmembrane domains (TMDs), nucleotide binding domains (NBDs), extracellular loops (ECLs), and intracellular loops (ICLs). Positions and distances were calculated using either in-house tcl scripts for VMD or plumed 2.8 [57].

Secondary structure calculations of the TM helices were performed using the cpptraj module [58] of ambertools using the *secstruct* function based on the DSSP algorithm [59].

The contacts of molecules (VIN, ENC or amino acids) were analyzed by Voronoi Laguerre Delaunay for Macromolecules (VLDM) [60]. VLDM relies on a tessellation method, that is, a partition of space into a collection of polyhedra filling space without overlaps or gaps. Delaunay tessellation and its Laguerre dual were performed using a set of heavy-atom cartesian coordinates and a weight that depends on the van der Waals radius of the atom, determined using the CHARMM36m force field. A contact occurs whenever two atoms share a common face in the tessellation. The interface between molecular groups is quantified by their polygonal surface area. Contact areas were calculated using VLDM and plotted using in-house R-scripts.

We also employed two advanced computational tools to unravel the intricate dynamics and allosteric communication pathways within the protein structure. Firstly, Bio3D [61], a comprehensive R package for the analysis of biomolecular structure, dynamics, and function, was utilized to calculate the cross-correlation of motions between different domains. This analysis facilitated the understanding of how movements in one domain of the protein could influence or correlate with movements in another, highlighting the interconnected nature of protein dynamics. Secondly, we used ALLOPATH [62,63], a specialized Python program based on network analysis, to identify and calculate allosteric pathways. ALLOPATH leverages the principles of network theory to map out the routes of allosteric communication across the protein, based on the MD simulation data.

MD simulation trajectories were visualized using VMD [64] and PyMOL [65]. 3D structure views figures were generated with PyMOL. Positions, distances, RMSD plots and probability densities, secondary structures and contacts plots were all generated using either R v3.6.1.

## 3. Results

We carried out classical MD simulations using three distinct transporter models representing the IF-open, IF-occluded and OF states (Fig. 1A). The IF-occluded and OF models were extracted from the PDB. The IF-open model, characterized by straight TM4 and TM10 helices and larger distances between NBDs, was taken from the AlphaFold database. Given the absence of experimental structures for this state for the human transporter in the PDB, we assumed its existence based on the presence of this conformation in the murine transporter and in the human ABCB4, which shares 75 % sequence identity [25,66–68]. Additionally, we constructed IF-open models in the presence of VIN, (Fig. S1) and IF-occluded models in the presence of ENC (Fig. S1). An overview of all the conducted simulations is provided in Table S1. For all these models, we analyzed the structural characteristics both in absence and in presence of the disordered linker segment to evaluate its influence on the dynamics and the substrate translocation process. Different initial conformations for the linker were generated in each state, a choice motivated by the significant uncertainty regarding the linker's position and conformation with respect to the other domains of the transporter. We hypothesized a large movement of this segment during the transition between various states.

Due to these considerations, we will present the results in separate sections. The first two sections will cover the results for the models without the linker, and the last section will cover the results for the systems incorporating the linker.

### 3.1. . Classical MD simulations in absence of the linker

#### 3.1.1. Structural features of the different P-gp state models

The structural characteristics of the constructed models were assessed in 3 replicas (1 ×300 ns + 2 ×100 ns) of classical MD runs by calculating the Cα RMSD, NBD1-NBD2 distances, TM4-TM6 distances and secondary structures of the TM helices. Larger RMSD fluctuations were found in the simulations of the IF-open conformation due to the larger separation between NBD1 and NBD2, starting with a distance of ~46 Å between their center of mass. In particular, some simulations in presence of VIN, showed the highest fluctuations with an averaged RMSD of 4.8 ± 1.3 Å and an averaged NBDs distance of 52 ± 5 Å. However slightly lower values are noticed when the NBDs uphold contacts with each other with an averaged RMSD of 4.5 ± 0.9 Å and an averaged NBDs separation distance of 43 ± 2 Å. For the simulations of the IF-occluded and OF states, where the NBDs are in closer positions, RMSD fluctuations were generally lower, with average RMSDs of 3.7 ± 0.8 Å and 3.6 ± 0.6 Å, respectively. The average distances between NBDs were 38 ± 1 Å for the IF-occluded state and 29 ± 0.7 Å for the OF state. A correlation of approximately 66 % was observed between the RMSD values and the separation distances of the NBDs across all three conformations, indicating that larger separations between the NBDs clearly contribute to higher RMSD values (Fig. S2). Additionally, multiple simulations of the IF-occluded conformation revealed a complete disruption at the TMDs/NBD2 interface, indicating significant instability in this region for this state (data not shown).

As previously noted, significant fluctuations in the separation distance between NBD1 and NBD2 were observed in the IF-open simulations considerably impacting the transporter's structure and dynamics. Remarkably, this variability is correlated with the distance between specific regions of TM4 (amino acids 235 to 239) and TM6 (amino acids 349 to 353) within the TMDs, which constitute the TM4-TM6 portal (Fig. 1 and S2). An important aspect contributing to the formation and opening of this portal within the TMD1 is the swapping of TM4/TM5 with respect to the other TM helices within TMD1 (Fig. 1A, left panel). This portal is suggested to serve as an entry point for ligands and lipids, as previously indicated by coarse-grained simulations of mouse P-gp [69]. Our observation indicates that this portal has the capacity to adopt a wider opening, possibly to accommodate the entry of compounds of various sizes. However, maintaining a certain separation distance between the NBDs might be crucial for the transporter's stability and function.

Another significant distinction among the different states of the transporter is the presence of either a kinked or straight helical conformation in the transmembrane (TM) helices, particularly noticeable in the TM4 and TM10 helices (Fig. 1A). Consequently, the conformational changes in P-gp, observed during its transitions between different states, result from the kinking and straightening of its TM helices. The secondary structure analysis along the MD trajectories showed that almost all transmembrane helices can exhibit kinking. The TM helices, except TM4, TM9, TM10 and TM12, exhibit possible kinks observable in all the three considered states (Table 1). On the other hand, TM4, TM9, TM10, and TM12 exhibit key kinks that are specific to each P-gp conformational state (Fig. S3): S238/F239 in TM4 marks the IF-occluded state; A819/N820 kink in TM9 appears in both the IF-occluded and IF-open states, with an extra bend near Q824 in the IF-open state, facilitating the formation of a 3–10 helix between these two kinks exclusively in this state; TM10 shows a large unstructured section in the IF-occluded state around S880 but maintains an alpha-helical structure in the IF-open and OF states; TM12 features specific turns in each state, indicating distinct conformational dynamics (Table 1 and Fig. S3).

Furthermore, noticeable local variations are found between the IF-open, IF-occluded and OF states, especially in these kinked regions (Fig. 1B). These variations may play a crucial role in the mechanisms of the functional cycle of P-gp. Notably, in the kinked region of TM4, TM10 and TM12, the side chains of W232, F239 (TM4), M876 (TM0) and F994 (TM12) exhibit varying orientations depending on the state. In the OF state, these residue side chains are oriented towards the lipid membrane. Conversely, in the IF-occluded state, the kinking of TM4 and TM10, along with the kinked TM12, positions these residues within the binding cavities. This configuration facilitates mutual contacts (Fig. 1B) and enables additional interactions with the ligands. In the IF-open conformation, the side chains of F239 (TM4) and M876 (TM10) are oriented towards the membrane, whereas the side chains of W232 (TM4) and F994 (TM12) are situated within the binding cavities. This arrangement suggests that the rotational dynamics of F239 and M876 play a pivotal role in the kinking and unkinking of TM4 and TM10, facilitating the transitions between the IF-open and -occluded conformations (detailed in the Enhanced Sampling section). Additionally, within the IF-open conformation, the W232 side chain demonstrates significant flexibility. Initially found in the binding pocket, it can easily rotate towards the membrane. Collectively, these data indicate that rotations of specific residue side chains play a crucial role in modifying the kinking and unwinding states of the TM helices, thus driving the conformational changes responsible for binding and release of the ligands.

#### 3.1.2. Phospholipids penetration from the TM4 / TM6 portal

In the IF-open models, we observed the entrance of phospholipids through the TM4/TM6 portal, which is proposed as an access point to the binding cavity [43]. In this state, both TM4 and TM6 helices retained their alpha-helical fold at the portal, resulting in the widening of the gateway at the inner leaflet of the membrane. In this context, W232, with its side chain situated inside the binding cavity, plays a key role in the selective attraction of phospholipids by engaging cation-pi interactions with the phospholipid headgroup (Fig. 2). These findings are in accordance with the known role of P-gp as a phospholipid floppase. This is further supported by structural data obtained from ABCB4, another phospholipid floppase, which shares 75 % sequence identity with P-gp. In ABCB4, the analogous W234 plays a key role in attracting and interacting with phospholipids [66].

Remarkably, in P-gp, the entrance of phospholipids remained possible even in the presence of VIN or ENC in the binding cavities (Fig. 2). In one simulation replica, in presence of ENC, W232 initially attracted a phospholipid within the binding cavity, and subsequently adjusted its side chain orientation to rotate toward the membrane. During this process, the phospholipid stayed within the binding cavity (Fig. 2B). On the other hand, no or less lipid entrance was noticed at the pseudo-symmetrical TM10/TM12 portal during the multiple conducted simulations. The observed absence of lipid penetration at the TM10/TM12 portal can be partially explained by the presence of E875 on TM10, which corresponds to the position of W232 on TM4. Moreover, TM10 keeps a tendency to form a kink around the S880 amino acid (as indicated in Fig. S3). This kinking action of TM10 narrows the gate and hinders the entry of lipids into the transporter from the TM10/TM12 portal.

**Table 1**
Kink regions in TM helices. State-dependent kink regions are highlighted in bold.

| TM1 | TM2 | TM3 | TM4 | TM5 | TM6 | TM7 | TM8 | TM9 | TM10 | TM11 | TM12 |
|---|---|---|---|---|---|---|---|---|---|---|---|
| G62 | | T176 | S222 | | S349 | G723 | T776 | **N820 Q824** G830 | A863 | L924 | **A980** |
| | | G185/7 | **S237/8** | | | | | | **S880** | | **A995** |
| | | | Y247 | | | | | | L890 | | |

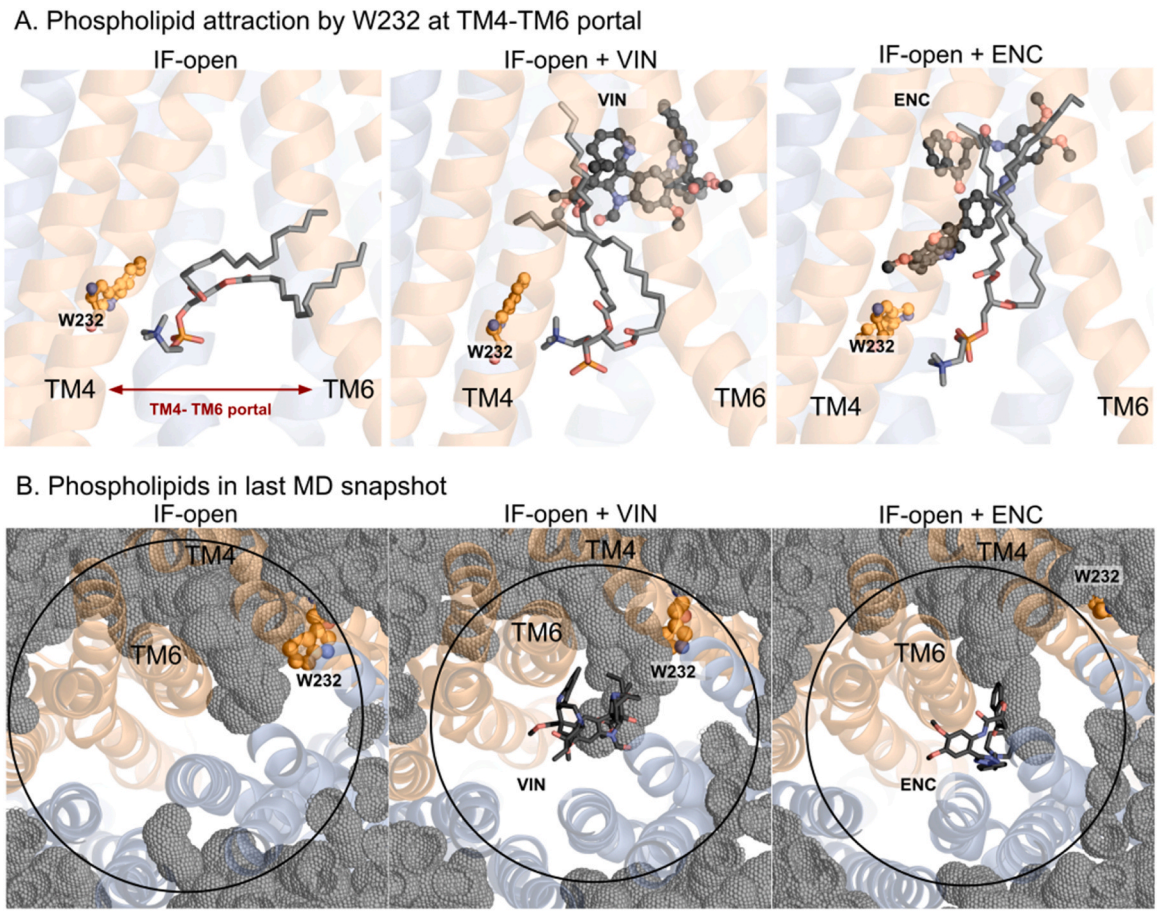


**Fig. 2.** The IF-open state allows the entrance of phospholipids. A) During the MD simulations of the IF-open conformation, phospholipids were drawn into the binding cavity through a cation-π interaction between the phospholipid headgroup and residue W232. This phenomenon was observed both in the absence of ligands (left panel) and in the presence of either a substrate (VIN, middle panel) or an inhibitor (ENC, right panel). In all cases, entrance of phospholipids was primarily observed through the TM4-TM6 portal. The protein is depicted in a transparent cartoon representation from a side view, with a zoomed-in focus on the TM4-TM6 portal. W232 in TM4, along with VIN and ENC molecules, are depicted in ball-and-stick representation, colored in orange and black, respectively. The attracted phospholipid is shown in gray sticks. B) Top views from the last MD snapshot illustrates phospholipid penetration into the binding cavity, observed in MD simulations in the absence of ligands (left panel) and in the presence of VIN (middle panel) or ENC (right panel). The protein is depicted in a transparent cartoon representation, with lipids displayed as gray pointed spheres. W232 in TM4 is shown in ball-and-stick representation and colored in orange. VIN and ENC are represented in black sticks.

In the IF-occluded state, both TM4 and TM10 exhibit kinks, resulting in the closure of both the TM4/TM6 and TM10/TM12 portals, thereby preventing any lipid entry (Fig. S4). A hallmark of the TM4-TM6 portal closure is the formation of a specific salt bridge between K234 and E353 on the respective helices (Fig. S4). The IF-occluded state could, thus, be regarded as a "locked" conformation that precedes substrate expulsion, thereby preventing its reentry into the cell, or an “inhibited” conformation when triggered by inhibitors.

In the OF state, the orientation of the W232 side chain is altered as it faces the membrane component, emphasizing the pivotal role of this residue’s rotation during the transport cycle. In this conformation, the transporter binding cavity is completely collapsed, effectively blocking the accommodation or the entry of any compounds. Collectively, these data indicate the multifaceted role of W232, not only in the conformational and functional cycle of P-gp but also in attracting various compounds, such as drugs or lipids, from the membrane.

### *3.1.3. Interactions of the substrate and inhibitor within the TMDs*

The cryo-EM structures of the human P-gp transporter, solved in an IF-occluded conformation, showed the presence of two overlapping binding sites stacked on top of each other for tariquidar-derived inhibitors (PDBs: 7O9W [22] (encequidar), 7A6C [21] (elacridar), 7A6E [21] (tariquidar), 7A6F [21] (zosuquidar)). In these structures both inhibitors come into contact, with the upper one forming a U-shaped fold, while the lower molecule forms an inverted L-shaped fold and extends towards the lower section of the membrane-spanning domains (Fig. 3A, top). In the presence of substrates, only the top binding site is occupied (PDBs: 7A69 [21] (vincristine), 6QEX [23] (taxol)) by one molecule still forming a U-shape (Fig. 3B, top). To better characterize the conformation of VIN (substrate) and ENC (inhibitor) within the TMDs, we built P-gp-ligands systems using the IF-open and IF-occluded conformations. For ENC, we opted to retain only the L-shaped, the more extended molecule.

Analysis of all classical MD simulations conducted in presence of ligands (VIN and ENC) revealed that a specific set of P-gp amino acids consistently interacts with the ligands regardless of the cavity occupied, and persists across both IF conformations: open and occluded. These common contacts involve TM5 (F303/I306/Y307/Y310), TM6 (F336/L339/F343/Q347), TM7 (Q725/F728), TM12 (F983/M986) (Fig. S5). The upper position of VIN in the IF-open conformation drives it to form additional contacts with TM1 (M69) and TM11 (Y953). The lower position of ENC in the IF-occluded conformation is stabilized by contacts with the kinked helices, TM4 (W232, I236 and F239) and TM10 (M876), as well as with TM12 (F994), TM5 (I299) and TM8 (F770) (Fig. S5).

ENC exhibits a notable flexibility within the IF-open models, adopting either a U-shape (Fig. 3A, bottom) or an extended

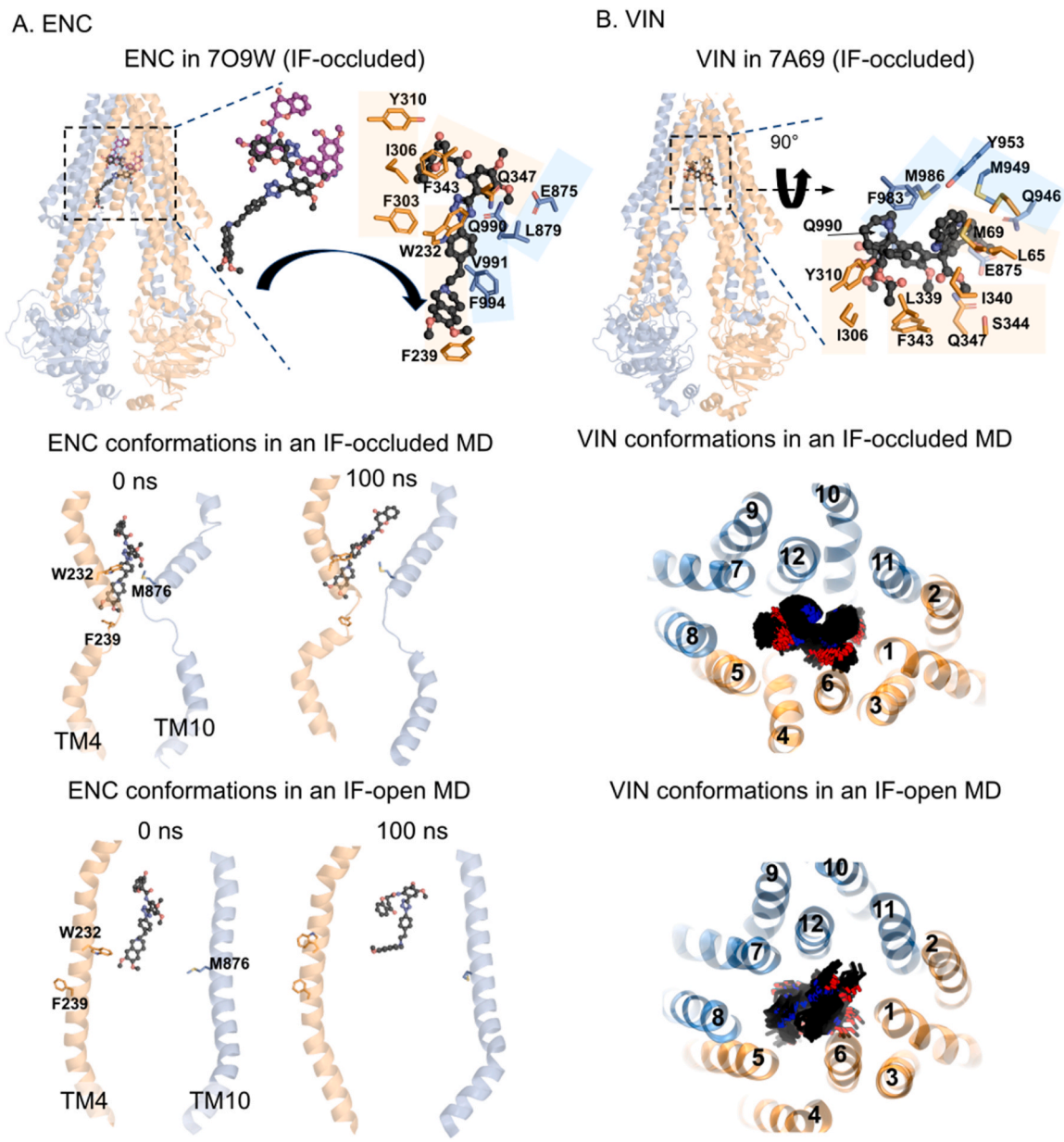


**Fig. 3.** Conformation and dynamics of ENC and VIN within the binding cavities of P-gp. A) Conformation of ENC within the IF-occluded cryo-EM structure (PDB ID 7O9W) (top and middle) and Alphafold model (bottom). Top panel: In 7O9W, two ENC molecules are present adopting a U-shape conformation (purple) and an extended L-shape conformation (black). Residues in contact with the L-shaped ENC are depicted in orange (TMD1) and blue (TMD2) sticks. Middle and Bottom panels: Evolution of ENC conformation (black) during classical MD simulations of the P-gp IF-occluded (middle) and IF-open (bottom) conformations. The initial conformation (0 ns, left) is shown, as well as the last snapshots from 100 ns-MD simulations. For clarity, only TM4 and TM10 are displayed in a transparent cartoon representation from a side view. B) Conformation of VIN within the IF-occluded cryo-EM structure (PDB ID 7A69) (top and middle) and Alphafold model (bottom). Top panel: In 7A69, VIN is found adopting a U-conformation (black). Residues in contact with VIN are depicted in orange (TMD1) and blue (TMD2) sticks. Middle and Bottom panels: VIN dynamics (black stick) during the MD simulations of the IF-occluded (middle) and IF-open (bottom) simulations. The TMD helices are shown from a top/extracellular view of P-gp. Different VIN conformations from each entire MD trajectory are simultaneously shown within the binding cavity.

conformation (not shown) across different simulations. In the first case, the upper section of the molecule is predominantly stabilized by TM5, TM7, and TM12, while the lower section exhibits a greater flexibility, primarily attributed to the loss of contact with W232. In the IF-occluded models, ENC's lower section benefits from enhanced stabilization through additional formed contacts with TM4 (W232) and TM10 (M876), thereby reducing its flexibility (Fig. 3A, middle).

On the other hand, VIN conformation is markedly more stable within both the IF-open and -occluded models. This stability is evidenced by consistent patterns of interaction across three replicated simulations of the inward-open conformation (Fig. S5). Here, VIN maintains an upper position within the transmembrane domains (TMDs), preserving a U-shaped conformation throughout all simulations (Fig. 3B, bottom). In the case of the IF-occluded state, VIN's stability is further enhanced through additional interactions with TM4 (W232) and TM10 (E875) (Fig. 3B, middle and Fig. S5).

The comparative analyses of the IF-open and -occluded conformations reveal distinct structural dynamics and functional implications for substrates and inhibitors. The IF-open conformation facilitates the entrance of ligands, characterized by a significant degree of flexibility, crucial for accommodating various ligands. These ligands engage contact with entering phospholipids in this state. In contrast, the IF-

occluded state represents a crucial transition conformation, effectively 'locking' the system. This locked conformation restricts further entrance of lipids or any other molecules within the binding cavities and stabilizes the ligands through specific additional interactions with kinked TM4 and TM10. This stabilization is crucial for the functional dynamics, suggesting a dual potential pathway: it could either progress towards facilitating the efflux process or lead to an inhibited state.

### 3.1.4. *Allosteric communication in P-gp various conformations*

To evaluate the synchronization of movements across the different domains of P-gp, we conducted a cross-correlation (CR) analysis using the Bio3D module [61] in R on MD simulations of each conformation. This analysis revealed the domains that are less or highly correlated as well as those that are anti-correlated (Fig. 4A). A significant difference was observed for the IF-open conformation compared to both the IF-occluded and OF conformations. Specifically, in the IF-occluded and

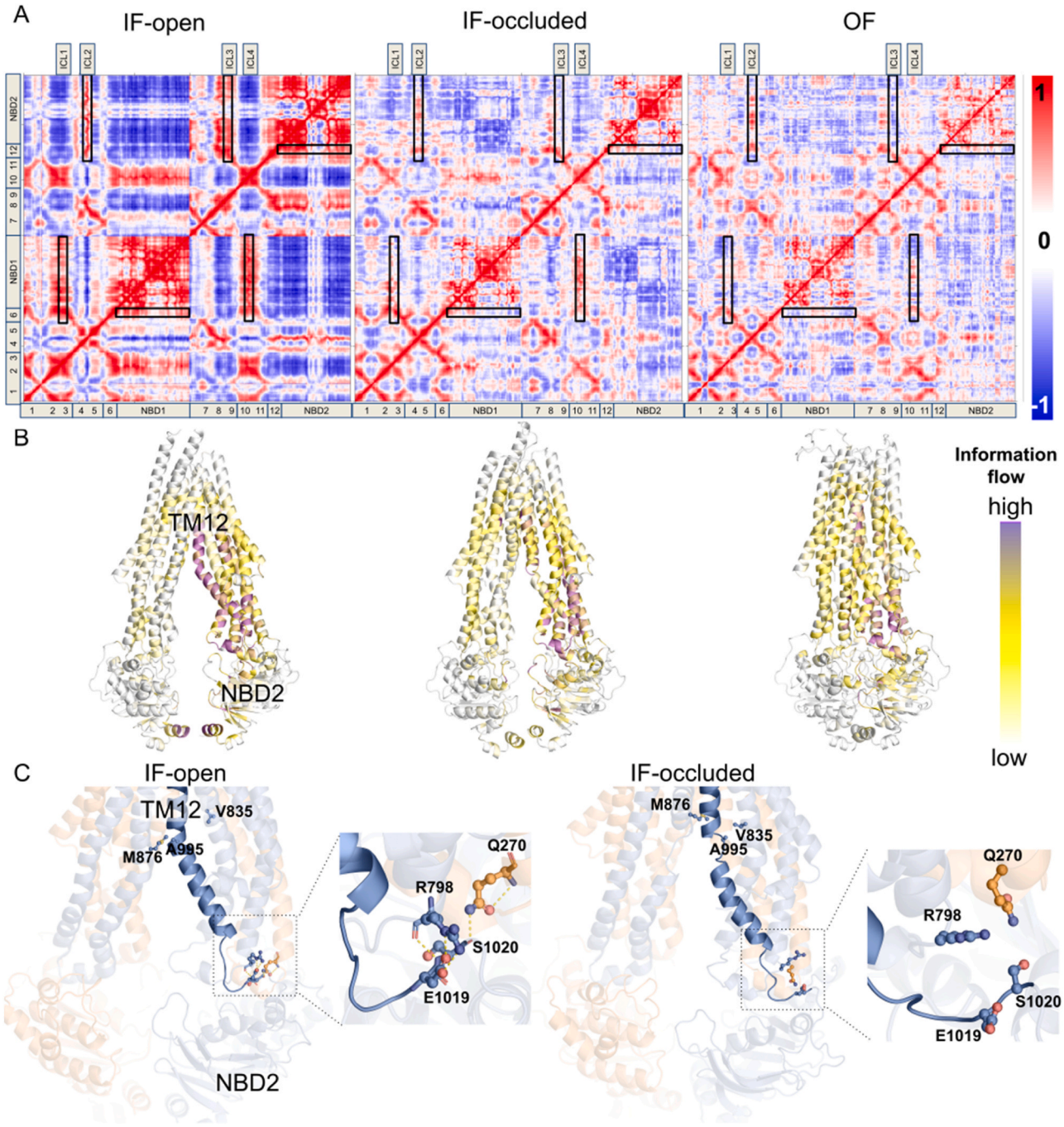


**Fig. 4.** Allosteric communication from the central binding cavity to the ATP binding sites. A) Using the Bio3D R package, dynamical cross-correlations (CR) were calculated from MD trajectories of the IF-open, IF-occluded and OF states, all in the absence of ligands. The Black boxes highlight the CR between the ICLs and NBDs (vertical boxes) and between TM6/TM12 and NBD1 and NBD2 (horizontal boxes). B) The information flow, calculated from MD trajectories, were projected on the Alphafold model of the IF-open state (left panel) and the IF-occluded (middle) and OF (right panel) cryo-EM structures of P-gp.These plots illustrate the dynamic allosteric pathways under different structural states. C) Visualization of TM12 contacts and conformations after 100 ns MD simulation: This panel contrasts TM12's behavior in the IF-open conformation (left panel) with that in the IF-occluded conformation (right panel). For enhanced clarity, only TM12 is highlighted while other regions of the protein are rendered transparent.

OF conformations, overall lower correlations were found, indicating a weaker communication between the TMDs and the NBDs. These results suggest a more effective communication between the TMDs and NBDs in the IF-open state, which may be crucial to initiate conformational changes after the binding of a ligand. In the OF state, due to the dimerization of both transporter' halves and the expulsion of the ligand, this communication could be no longer needed. ATP hydrolysis would then induce the NBDs separation, leading back to the IF-open state. Nevertheless, the results observed for the IF-occluded conformation are particularly intriguing, as they also indicate a loss of communication. This could imply that the IF-occluded conformation represents an inhibited state. The CR analysis highlighted that while TMD1 and NBD1, as well as TMD2 and NBD2, move in sync (positive correlation), ICL2 and ICL4 diverge from their adjacent NBDs (negative correlation), indicating opposite movements (Fig. 4A). These ICLs show a positive correlation with the opposite NBDs (ICL2 with NBD2 and ICL4 with NBD1), attributed to the domain-swapped structure of TMDs and the cross-domain interactions of these regions (see Fig. 1A). Importantly, the analysis pointed out a decrease in correlation between the ICLs and NBDs in both the IF-occluded and OF states (Fig. 4A, vertical black boxes and horizontal black boxes).

The observed CR variations between the IF-open and the IF-occluded / OF states prompted us to investigate the allosteric communication between the central binding cavity and the NBDs using the AlloPath program [62,63]. This method employs network analysis on MD simulations, and calculates allosteric pathways across each state based on the information flow (InF) at each residue (methodological details in [62, 63]). This analysis revealed a consistent contribution from several residues (e.g. W162 in ICL1 and residues in TM6) (Fig. S6) in mediating communication between the central binding cavity and NBD1 across the IF-open and -occluded states (Fig. S6). Nonetheless, a distinct divergence in the involvement of these residues became evident in the OF state, highlighting a shift in the mechanism of allosteric communication (Fig. S6). In contrast, the communication between the central binding cavity and NBD2 showed a markedly different scenario. In the IF-occluded state, TM12 displayed a marked decrease in InF values, contrasting with the IF-open and OF conformations (Fig. 4B and S6), highlighting an asymmetrical communication between the central binding cavity and the two NBDs. Notably, the reduced involvement of TM12 in the communication with NBD2 in the IF-occluded state could be a key factor in P-gp inhibition mechanisms. Indeed, the IF-occluded state is characterized by significant structural alterations, notably the kinking of TM4 and TM10 and the binding of an inhibitor within the lower binding cavity, impacting the interaction interface with NBD2, by altering key contacts in these regions.

By employing the Demystifying program [70], which leverages machine learning and deep learning techniques to analyze MD simulations of distinct conformations, we were able to identify the most crucial residues that exhibit differential behavior across each conformational state. Demystifying analysis highlighted two specific regions: A995 in TM12 and S1020 at the TM12/NBD2 junction. A995 showed distinct orientations between the IF-occluded and IF-open states affecting the conformation of TM12 and subsequently the ICL2/ICL3/TM12/NBD2 interfaces. In the IF-occluded state, A995 interacts with V835 (TM9), whereas in the IF-open state, it contacts M876 (TM10) (Fig. 4C). The TM12/NBD2 junction, around residue S1020, is crucial for maintaining the structural cohesion necessary for the proper function of P-gp. Notably, in the IF-open state, a salt bridge between D1019 and R798 (in ICL3) alongside a hydrogen bond between the main chain of S1020 and Q270 (in ICL2) stabilizes this interface. However, the IF-occluded state's altered TM12 conformation disrupted these critical interactions, underscoring the importance of this interface on the transporter's global structure and dynamics (Fig. 4C).

To conclude, in the IF-occluded conformation, the resultant effect of kinked TM4 and TM10, alongside inhibitor binding, on TM12's conformation, thereby impacts the lower part of the interface between the TMDs with NBD2, potentially inhibiting the conformational cycle of P-gp. This proposed inhibition mechanism gains further credence from two independent studies [71,72], suggesting the presence of binding sites for non-competitive inhibitors, specifically flavonoids, at this interface, indicating a strategic point of intervention for modulating P-gp activity.

### 3.2. *Enhanced sampling to drive conformational transitions and substrate translocation in the models lacking the linker*

To model the transitions between the different conformations, we carried out ketMD (kinetically excited targeted MD) and ABMD (Adiabatic Biasing MD) simulations (summarized in Supplementary Table S1), as detailed in the methods section.

#### 3.2.1. *ketMD simulations*

The ketMD simulations effectively captured the global transitions between the IF-open and OF states, characterized by the canonical straight conformations of TM4 and TM10 helices. The final RMSD values from the target were approximately 2.5 Å for the transition from OF to IF-open and for the transition from IF-open to OF, indicating a high level of accuracy in modeling these conformational changes (Fig. 5A, S7 and S8). Overall, ketMD succeeded in simulating these global movements. However, some specific localized dynamics were not precisely modeled. Differences were observed between the targeted structures and the final ketMD models in the position of the side chain of W232 as well as the openness /closure of the binding cavity (Fig. 5A and S7-A).

Notably, the presence of ENC during the transition from IF-open to IF-occluded promoted the kinking in TM4, indicating that inhibitors might facilitate achieving the IF-occluded conformation (Fig. 5B and S9). As expected, ketMD simulations confirmed that TM4 kinking/unkinking process is triggered by F239 whose side chain can adopt two different orientations, either located within the binding cavity in the IF-occluded state or facing the membrane in the IF-open conformation (Fig. S7-B). On the other hand, TM10 demonstrated a natural tendency to kink at S880/G881, a behavior consistently observed in classical MD simulations as well. However, straightening both TM4 and TM10 from the IF-occluded back to IF-open was hardly feasible and required the usage of a higher kinetic excitation (Fig. 5B and S9). Furthermore, during the transition from IF-occluded to OF, straightening these helices proved more challenging once the NBDs had dimerized, suggesting that helix straightening may be a prerequisite for NBD dimerization and essential for achieving a properly formed OF conformation (Fig. 5C and S7-C). Conversely, the separation of NBDs during the transition from OF to IF-occluded facilitated the initiation of kinking in TM4/TM10, supporting the hypothesis that NBD dimerization prevents the kinking process (Fig. 5C and S7-C).

Through analysis of ketMD results, we have identified significant structural distinctions between IF-occluded and OF states. In the OF conformation, TM6 and TM12 are in close contact, effectively sealing the transporter's cavity. In contrast, the IF-occluded state is characterized by a separation of TM6 and TM12, with the cavity becoming obstructed by kinked TM4 and TM10 instead. Therefore, the transition from the IF-occluded towards the OF state necessitates first the separation and subsequent straightening of TM4 and TM10, which would then favor the interaction between TM6 and TM12 as achieved in the OF state. Based on these findings, we suggest that P-gp must first adopt an inward "straight" TM4/TM10 state before progressing to the OF conformation. Consequently, we may speculate that the IF-occluded state may not serve as an intermediate step preceding ligand expulsion but might instead represent a "blocked" or "inhibited" state of P-gp. It is noteworthy to remind that all IF-occluded structures have been determined in the presence of an inhibiting antibody fragment, such as the UIC2 Fab-fragment in our structure derived from 7O9W. This fragment specifically binds to P-gp at the extracellular loops (ECLs), obstructing the efflux of substrates and inhibitors. The IF-occluded conformation

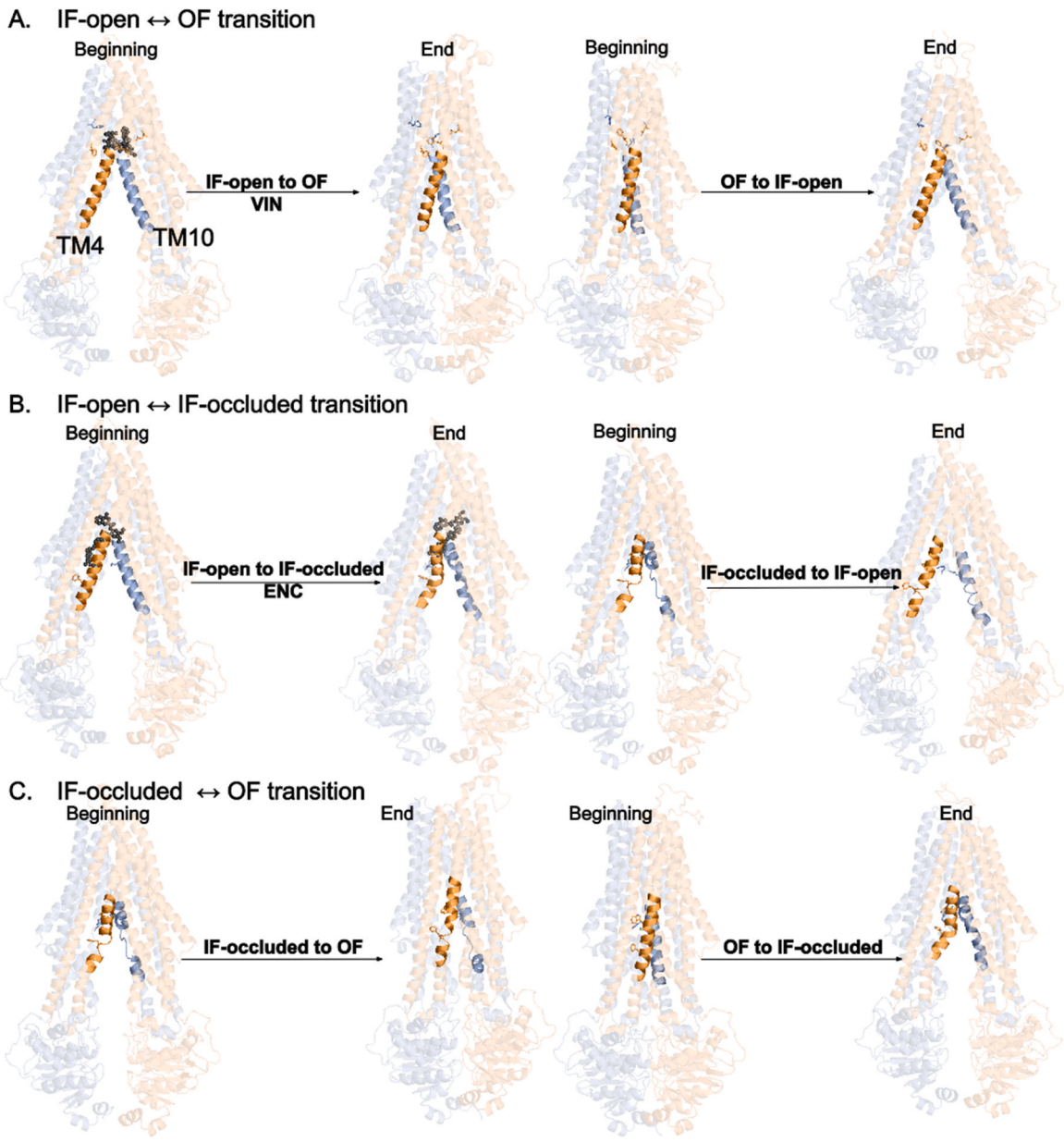


**Fig. 5.** ketMD simulations of the P-gp state transitions. First and last snapshots of ketMD simulations are depicted for each transition between the P-gp states. Transitions between the IF-open and OF (A), the IF-open and IF-occluded (B), and the IF-occluded and OF states were explored either in presence or absence of a ligand (inhibitor: ENC, substrate: VIN represented in black ball and stick representation). For clarity the whole protein is shown in transparent cartoon representation, except for TM4 and TM10 segments, where kinking and/or unkinking events drive the conformational changes.

may be thus specifically induced by the interaction with this antibody fragment.

### 3.2.2. *ABMD simulations*

Given that ketMD encountered limitations in reproducing certain local changes during the different transitions, we supplemented our study with ABMD simulations. Unlike ketMD, ABMD simulations necessitate the identification of relevant collective variables (CVs) that effectively drive the transitions between initial and final states. To induce specific local alterations, a ratchet-like harmonic potential is introduced in the simulation, propelling the CVs towards the desired target [56]. Our comparative analysis of the IF-open and OF conformations enabled us to identify crucial salt bridges that are instrumental in the dimerization of the transporter halves, thereby stabilizing the OF conformation during the transition from the IF-open state. These salt bridges are located at the interfaces of NBD1/NBD2, NBDs/ICLs, and between the TM helices region just beneath the lipid bilayer. Notably, the segments of the TMDs within the membrane region were found to lack salt bridges. Transitioning between states, therefore, necessitates the formation and disruption of these salt bridges, culminating in the establishment of new, state-specific salt bridges. The key state-specific salt bridges identified in our investigation are summarized in Table 2 and depicted in Fig. 6A. The usage of these salt bridges as CVs in ABMD allows us to generate proper transitions between IF-open and OF conformations (Fig. S10). However, transitioning from the OF to the IF-open state presented greater challenges, as it necessitated the disruption of large interfaces between the TMDs and the NBDs.

Moreover, transitioning between the IF-open, occluded, and OF conformations also required the strategic repositioning of specific amino acids. The pseudo symmetrical residues from TMD1 and TMD2 crucial for these transitions are depicted in Fig. 6B. Including these alternative positions as CVs in ABMD successfully facilitated the reproduction of

**Table 2**
List of salt-bridges (S) specific to each conformational state (columns 1–3) and list residues exhibiting state-dependent positioning changes (column 4).

| IF-open specific SB | IF-occluded specific SB | OF specific SB | State-dependent residues |
|---|---|---|---|
| K249-E283 (TM4-TM5) | K234-E353 (TM4-TM6) | K189-D997 (TM3-TM12) | W232 (TM4) |
| K291-E243 (TM5-TM4) | K934-E889 (TM11-TM10) | K249-E170 (TM4-TM3) | F239 (TM4) |
| R817-D821 (TM9) | | K291-E353 (TM5-TM6) | R832 (TM9) |
| K887-E891 (TM10) | | R359-D241 (TM6-TM4) | E875 (TM10) |
| K934-D886 (TM11-TM10) | | K887-D821 (TM10-TM9) | M876 (TM10) |
| K1172-D1124 (NBD2) | | R817-E891 (TM9-TM10) | Q882(TM10) |
| | | K934-E184 (TM11-TM3) | F994 (TM12) |
| | | K1000-D886 (TM12-TM10) | |
| | | K1172-D902 (NBD2-ICL4) | |
| | | K536-E1119 (NBD1-NBD2) | |
| | | K1181-E476 (NBD2-NBD1) | |

transitions between the IF-open and -occluded conformations, as well as the transition from IF-occluded to OF. However, the transition from OF to IF-occluded proved to be more challenging with the identified CVs, suggesting the necessity for an alternative pathway. This difficulty may also imply that the transition from OF to IF-open is energetically more favorable than shifting to the IF-occluded state, highlighting the intricate energy landscape governing the P-gp conformational changes.

#### 3.2.3. *Translocation of the substrate: VIN exit pathway*

The ketMD and ABMD simulations also allowed us to investigate the translocation pathways of VIN, starting from its initial position within the binding site and tracing its movement until it exited from the protein. Thus, in both cases, we simulate the transition from the IF-open state to the OF state, which includes the transport of VIN out of the transporter.

In fact, at the outset, classical MD enabled the characterization of VIN's binding site by identifying the key transmembrane (TM) regions and residues interacting with VIN within the site (see previous sections and Fig. S5). Both ketMD and ABMD simulations have now permitted the identification of new common residues that contact VIN prior to its exit from the transporter. These new regions encompass the upper portions of TM1 (F72,M75,T76,F79), TM2(Y118), TM5 (F314), ECL3/TM6 (I328,L332, F335), TM7/ECL4 (A729,F732,S733,I736,F739, T740), TM11 (F957) and TM12 (F971, L975) (Fig. 7A).

Nonetheless, some differences exist between the results yielded by ketMD and ABMD simulations. It is important to be cautious in interpreting the frequency differences of contacts in Fig. 7A, as it depends on the simulation length and the duration VIN stays inside versus outside the protein. In ketMD simulations, the TM and ECL regions undergo early conformational changes to align with the OF target conformation before the ligand ascends, facilitating VIN's exit through a central path without contacting the ECLs, in particular ECL1 (Fig. 7A). In contrast, the ABMD simulations showed that VIN came first to make contacts with the ECLs, particularly ECL1, which subsequently adjusts to assist VIN's exit, leading to more specific contacts, especially with ECL1, and to a lesser extent with ECL4 and ECL6 (Fig. 7A). In these simulations, an eccentric exit path for VIN bordered by upper TM1, TM2, TM6, TM7, TM11, and TM12, is instead identified (Fig. 7B). Both ketMD and ABMD, highlighted the critical role played by ECL1 dynamics, marking it as the pivotal gateway for VIN's translocation. These computational insights are in agreement with experimental evidence, which demonstrates that cysteine cross-linking ECL1 to ECL4 (A80C/R741C) when the transporter is in its IF-open conformation effectively inhibits drug efflux and ATPase activity [73].

### 3.3. . *Modeling of P-gp in presence of the linker*

In this study, a particularly challenging task was predicting the conformation of the linker (amino acids 630–695) connecting the NBD1 to the TMD2 within P-gp. This region poses a substantial challenge for conventional loop prediction methodologies due to its size. Its structural conformation has remained unresolved by cryo-EM techniques, attributed to its high degree of flexibility and lack of stable secondary structures. Some human P-gp models, which include the linker, have been proposed using homology modeling [74,75] and MD simulations [76–78]. Notably, the Dos Santos group contributed to this work [79,80]. Their models were predicted for the IF-open conformation of the transporter, with the linker positioned between the two halves, particularly at the NBD1-NBD2 interface. However, it is important to note that this position is not expected to be conserved. During the transition towards the OF conformation, the linker should be displaced to permit the proper NBD1/NBD2 dimerization.

AlphaFold2 was able to predict a full-length model of P-gp in the IF-open state (AF-P08183-F1), including the linker (Fig. 8A). Yet, the per-residue confidence score provided by AlphaFold for the linker was relatively low (pLDDT $< 50$). That reflects some uncertainty in the prediction of the linker conformation. Another limitation of AlphaFold was its inability to predict models including the linker for the IF-occluded and OF states of P-gp. For these states, our primary focus was on modeling the linker region, as the rest of the protein (the TMDs and NBDs) were obtained experimentally by cryo-EM. To address this gap, we employed iTasser to construct several linker models within these states (Fig. 8A). The diversity of models generated underscored the difficulties in accurately modeling this segment, as many models ranked within the top five displayed clashes between the linker and other domains of P-gp. To mitigate these issues, we selected one distinct linker model per state that did not exhibit clashes or problematic conformations relative to other domains. Consequently, each state model showcased a unique conformation of the linker.

In the AlphaFold model of the IF-open state, the linker spans between the transporter's two halves, notably between the ICLs and the NBDs. The C-terminal linker segment (aa 680–695) forms an alpha-helical structure, establishing interactions with TM10 (L884-L688 / E891-K685), ICL1 (D177-K681), and ICL3 (R817-E686). This generated configuration is likely influenced by the presence of a similar alpha-helical structure in the regulatory (R) domain of the inward-facing apo state of CFTR (ABCC7) as observed by cryo-EM [29,81]. Meanwhile, the portion spanning from aa 630 to 680 aligns along the interface between the NBDs, engaging frequently with ATP2 and its respective binding site within NBD2 (Fig. 8A). MD simulations of this full-length IF-open state revealed a slightly more stable RMSDs as compared to the systems simulated in absence of the linker (Fig. S11). The linker itself exhibited a wide range of flexibility, with RMSD fluctuations ranging from approximately 4 Å to over 25 Å. Overall, these findings indicate the significant impact of the linker on the structural stability and dynamics of the transporter.

During classical MD simulations carried out in presence of the linker, an interesting event occurred: a cholesterol (CHOL) molecule penetrated the binding cavity (Fig. 8B), ultimately reaching a position close to that of VIN (Fig. 8C). Initially attracted to the portal formed by TM4 and TM6, the CHOL molecule's trajectory highlights a plausible pathway for ligand entry into P-gp, suggesting a potential entry mechanism facilitated by the interaction with these TM helices. Interestingly, in the ketMD simulation modeling the transition from OF to IF-open states, a similar entry pathway for CHOL was observed (Fig. 8D), further reinforcing the hypothesis that this region plays a crucial role in the entry process. Initially, in the OF state, TM6 was inaccessible due to the positioning of TM3 in the front. However, as the transition progressed,

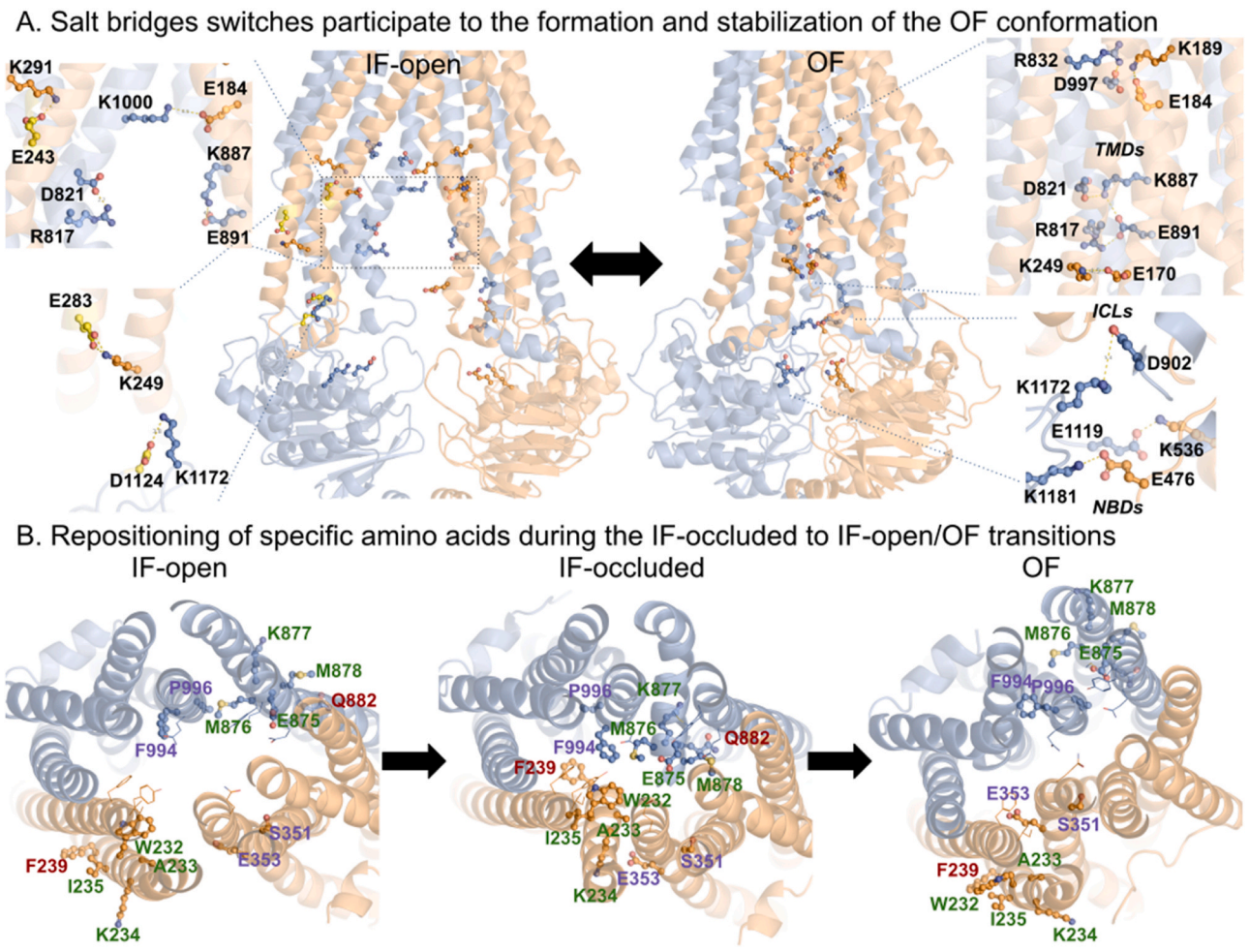


**Fig. 6.** P-gp conformational changes involve salt-bridges switches and specific amino acids repositioning. A) Salt-bridge analysis across P-gp states highlighted their crucial role in domain dimerization and stabilizing the OF state. Their disruption enables a return back to the IF-open state, characterized by the formation of alternative salt bridges. P-gp is depicted using a transparent cartoon representation, amino acids that participate in salt-bridge formation in both the IF-open and OF states are displayed either in orange or blue ball-and-stick representation. Amino acids that are specifically found in forming IF-open bridges are distinctly highlighted in yellow. The salt-bridges identified by this analysis were thus used as CVs during the ABMD simulations for the IF-open / OF transitions. B) Specific amino-acids rearrangement also contribute to P-gp conformational changes. While some amino acids are crucial for ligand accommodation within the binding cavities (not depicted here, see Fig. A.5. for details), others (represented in ball and stick) play roles in ligand recruitment and facilitation of conformational transitions. The repositioning of the residue side chains was used as CVs in the ABMD simulations to model the transitions between the different P-gp states. For enhanced clarity, the protein is presented in a transparent cartoon representation from a top view. Crucial amino acids are displayed in ball-and-stick representation, with similar colors assigned to corresponding residues in TMD1 and TMD2.

TM6 became accessible, which facilitated the binding of CHOL to the TM4/TM6 portal and its subsequent entry into the binding cavity. In summary, the integration of classical MD and ketMD simulations underlined the TM4-TM6 portal's pivotal role in ligand entry into P-gp. The recurrent entry of cholesterol (CHOL) across various states highlights this pathway's significance in P-gp's functions, offering crucial insights into possible ligand processing mechanisms. These insights align with a study that suggests that P-gp facilitates membrane cholesterol redistribution, linking the stimulation of its cholesterol-induced ATPase activity with cholesterol translocation [82].

Nevertheless, in the AlphaFold model of the IF-open state, the positioning of the linker spanning between the transporter halves presented challenges during the ketMD (and some ABMD) simulations aimed at modeling the transition from the IF-open to the OF state. To reach the OF/NBDs closed conformation in the transporter, it was imperative for the linker to be repositioned away from the interface between NBD1 and NBD2. Such relocation of the linker did not occur during the ketMD simulations (Fig. S12-A, left panel) and multiple ABMD simulations were performed to achieve the breaking of the contacts between the alpha-helical region of the linker and the ICLs and the NBDs in order to dislodging the linker from the cavity formed between the ICLs and NBDs (Fig. S12-B, left panel). For the transition from the OF to the IF-open state, the positioning of the linker on the surface of the intracellular domains resulted in fewer complications (Fig. S12 and S13). These results illustrated the crucial role of the linker segment's position in the structural rearrangement necessary for ATP binding site formation. Regarding substrate transport, both ketMD and ABMD simulations including the linker, identified transport pathways for the substrate similar to those observed in simulations conducted without the linker (Fig. S14).

## 4. Discussion

In this study, we employed classical and enhanced MD simulations to elucidate the structural and functional dynamics of P-gp. Our advanced simulations, specifically kinetically excited targeted MD (ketMD) and adiabatic biasing MD (ABMD), provided new insights into the conformational states and translocation mechanisms of P-gp, which plays a crucial role in cellular detoxification and drug efflux.

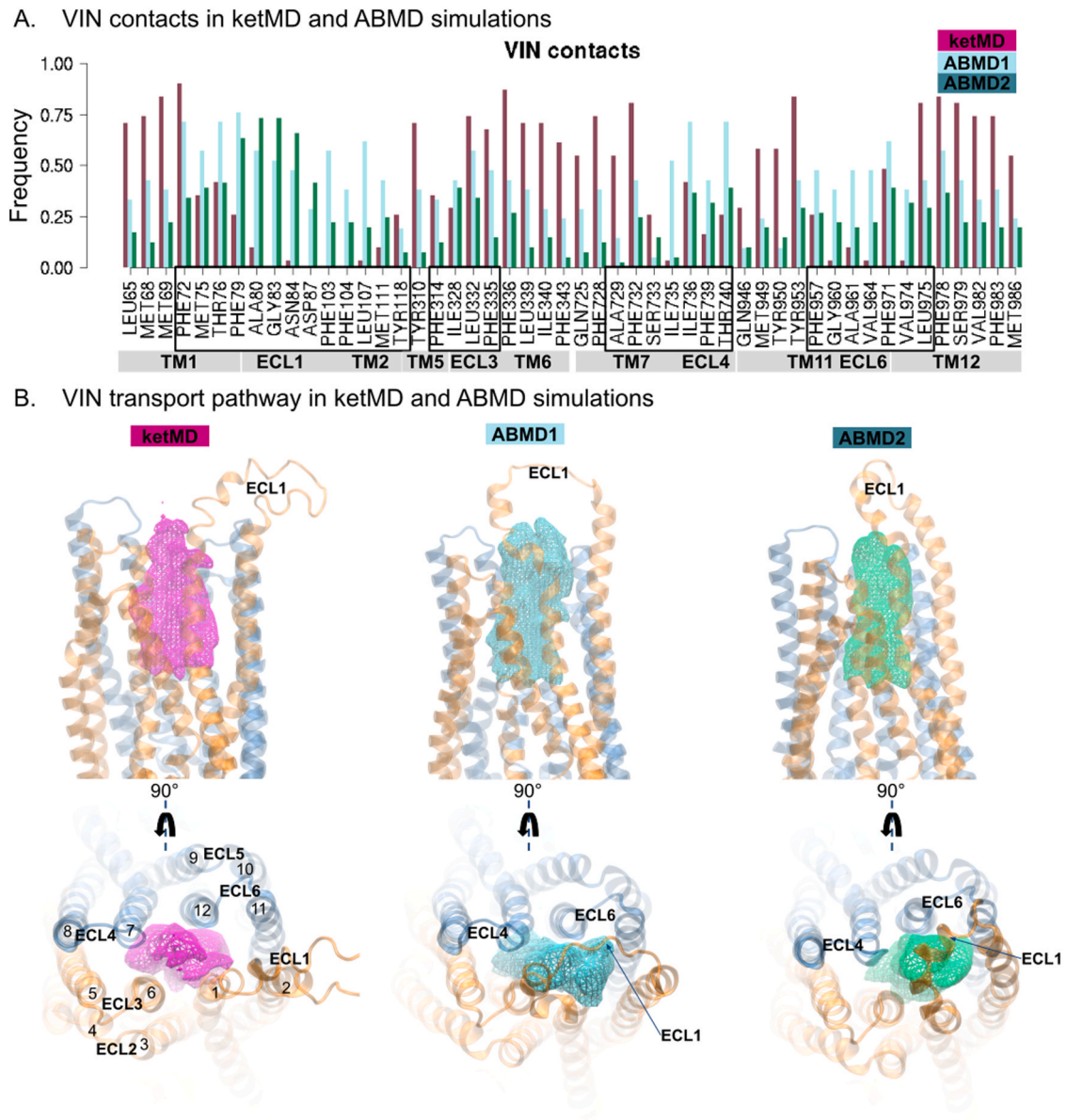


**Fig. 7. Observation of VIN translocation during one ketMD and two replicas of ABMD simulations.** A) Contact analysis: The contact frequencies between VIN and surrounding residues as it translocates out of P-gp were calculated over ketMD and ABMD simulation trajectories. B) Visualization of VIN occupancy density: The density of VIN's occupancy throughout the simulations was calculated with the Volmap tool in VMD for both ketMD and ABMD trajectories. The resulting data are visualized as mesh isosurfaces (at an isovalue of 0.009), with both side and top views provided to offer comprehensive spatial understanding. To ensure focus on the VIN occupancy, the protein is depicted in a transparent cartoon representation, allowing for clear visibility of VIN's pathways within P-gp.

### *4.1. Kinking/unkinking of the TM helices*

Our simulations demonstrated the critical role of kinking and unkinking of the transmembrane helices in state transitions, particularly the role of TM4 and TM10 unkinking in achieving the OF conformation of P-gp. Cryo-EM structures of human P-gp in the IF state consistently showed an occluded conformation with kinked TM4 and TM10, whether in the presence of substrates or inhibitors [21–23]. Interestingly, while most murine P-gp structures were found in an IF-open state (with straight TM conformations), kinked conformations for TM4, but not for TM10, were observed in some X-ray crystallography structures of murine P-gp only upon binding of ligands that activate ATPase activity [83].

Our simulations suggest that the unkinking of these helices, which act as flexible hinges preventing substrate reentry [84], facilitates the conformational shifts from IF to OF states. Previous studies using targeted MD simulations to explore the P-gp IF to OF transition reported extensive TM rearrangements but did not observe any kink or distortion events in TM4 and TM10 [77,85,86]. Our findings suggest that stabilizing the kinked state could inhibit P-gp, by potentially destabilizing the communication between the TMDs and NBD2 (Fig. 4). Other studies have suggested that some natural compounds (flavonoids) could indeed target this TMDs/NBD2 interface and induce P-gp inhibition [71,72]. We thus propose that designing inhibitors to stabilize this IF-occluded conformation and impede P-gp function could be a potential strategy to target MDR.

It is important to note that structural modifications during the cryo-EM process, including mutations at the NBD catalytic residues to trap P-gp in an OF state [24] and the usage of inhibitory antibody fragment bound to the external side of the transporter [21] to promote protein stabilization and trapping in IF conformations, may induce significant changes in P-gp structure and function, potentially leading to erratic

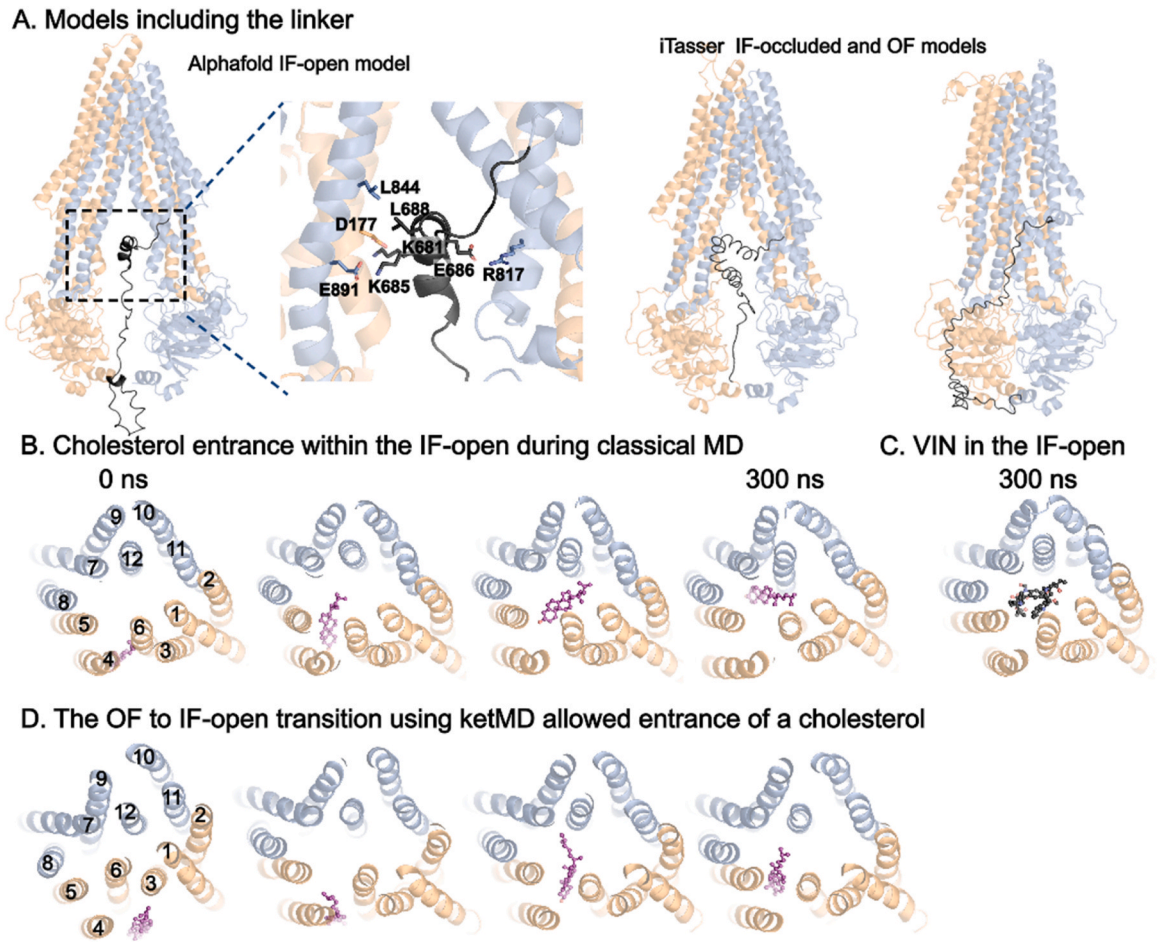


**Fig. 8.** Modeling of P-gp in presence of the linker. A) Models including the linker domain: The IF-open conformation was based on the AlphaFold model, while iTasser was used to generate IF-occluded and OF conformations that include the linker domain. Side views are provided for all models to offer a comprehensive perspective. Additionally, a zoomed-in view highlights the interaction of the alpha-helical C-terminal segment of the linker domain, an interaction uniquely formed in the AlphaFold model. B) Cholesterol entry in the IF-open conformation: During standard MD simulations of the IF-open state with the linker domain and without ligands, cholesterol entry into the binding cavity was observed. The progression of cholesterol's position is depicted along the MD simulation trajectory. C) Final snapshot with VIN: View of the last frame from a 300 ns classical MD simulation with the linker in the presence of VIN, highlighting the structural context in presence of the linker domain. D) Cholesterol entry in ketMD simulation: The entry of cholesterol into the binding cavity was also observed during a ketMD simulation of the transition from the OF to the IF-open state, with the linker domain present and no ligands. B-D)The binding pocket is visualized from a top view, with the protein depicted in a transparent cartoon representation for clarity. VIN and cholesterol molecules are shown in black and purple ball-and-stick representations, respectively.

conclusions. A cryo-EM structure of murine P-gp bound to ivacaftor [25] obtained without any structural modifications or antibodies revealed straight helical conformations of TM4 and TM10. These results highlight the importance to carefully consider the experimental conditions to avoid misinterpretations.

### 4.2. Dynamics of the NBDs

Our simulations also revealed an asymmetric behavior in ATP binding, with a less stable binding within the NBD2 (data not shown). This agrees with previous experimental studies that reported ATP binding and hydrolysis are not symmetrically distributed between the two NBDs [33,76,87]. Furthermore, our analysis showed significant asymmetry between NBD1 and NBD2 dynamics. Previous MD studies have shown higher flexibility within both NBDs during classical MD simulations in presence of active molecules (substrates and inhibitors), but not with non-active molecules [84,88]. Our comparison of apo simulations with those in the presence of VIN or ENC also revealed larger root mean square fluctuation (RMSF) in ICL2, ICL3, at the TM6/NBD1 and TM12/NBD2 junctions, and in NBD2 in presence of VIN or ENC (Fig. S15). Interestingly, ICL2 and ICL3, together with NBD2, form a hydrophobic transmission interface that Loo and Clarke studied using cross-linking experiments, finding it to be critical for proper folding and activity [89].

Finally, our data showed that the NBD1-NBD2 in the IF-open conformation can reach very large distances, up to ~ 60 A, leading to very large RMSD with respect to the initial AlphaFold model. This observation highlighted the highly flexible nature of the IF-open state compared to the IF-occluded and OF states. The Alphafold IF-open could thus be considered as an unstable state. Nevertheless, the NBD-NBD distances reported in the literature for murine P-gp structures in the IF-open conformation further support the high conformational flexibility of the transporter. These distances range from ~30 Å (PDB ID: 3G5U [67]) to ~60 Å (PDB ID: 5KPJ [33]), in accordance with our findings. We thus suggest that this high degree of flexibility could be a crucial aspect of P-gp's function, allowing it to accommodate various sizes of substrates and inhibitors.

### 4.3. Ligand binding and translocation

Our study provided detailed insights into the binding contacts and conformational stability of VIN and ENC within their distinct binding site (Fig. 3 and Fig. S5). The identified P-gp residues interacting with these ligands underscore the polyspecific nature of P-gp binding pockets.

Hydrophobic amino acids, particularly PHE, constituted the majority (more than 70 %) of the residues in contact with the ligands. Additionally, for the upper binding site where VIN binds, MET residues made a notable contribution. Polar residues, including GLN and TYR, comprised around 30 % of the interacting amino acids. These results are consistent with previous experimental and MD studies [28,68,75,85,90]. Two key residues on the kinked TM4 and TM10 helices were identified: W232 on TM4 and E875 on TM10. E875, the only acidic amino acid, can form salt bridges with positively charged nitrogens of the ligands only in the IF-occluded state (see Fig. S16). It has been proposed in a study, combining experimental and MD approaches, to potentially contribute to the inhibition mechanism by forming H-bond with carnosine, an endogenous dipeptide suggested to inhibit P-gp activity [91]. On the other hand, W232 appears to recruit and stabilize ligands within the binding pocket, a mechanism similar to that observed for the phospholipid translocation process of ABCB4, sharing 75 % of sequence identity with P-gp [66]. Additionally, our study showed that VIN and ENC could interact with attracted lipids by W232 within the binding cavity in the IF-open state, showing the capacity of this transporter to accommodate several molecules simultaneously through the apparition of multiple flexible binding sites (Fig. 2), a feature previously suggested by several experimental and structural studies [92].

Additionally, our enhanced MD simulations revealed the translocation pathways for VIN, elucidated through ketMD and ABMD simulations. These simulations highlighted the significant contribution of newly identified hydrophobic amino-acids (around 75 %), with PHE residues making up to 27 % of all residues newly found (Fig. 7 and Fig. S14). The simulations indicated the critical role of the ECLs, particularly ECL1, in facilitating ligand exit. This observation aligns with experimental evidence showing that blocking ECL1, through the formation of a disulfide bond with ECL4, inhibits drug efflux and ATPase activity, underscoring its importance in the translocation process [73]. Ultimately, the newly identified residues participating in the translocation process of substrates open avenues for experimental validation and provide potential targets for therapeutic intervention aimed at modulating P-gp activity.

### 4.4. Role of the linker region in P-gp dynamics

The flexibility and disordered nature of the linker region are crucial for the proper assembly and function of P-gp, potentially mediated through post-translational modifications [20,31,32,93]. Ford et al. emphasized the importance of linker regions in ABC transporters, highlighting their role in ensuring proper protein assembly, promoting correct folding, and facilitating functional interactions. They also discussed the evolutionary and functional diversity of linker regions, suggesting that these regions are not merely structural connectors but play active roles in protein regulation [93]. Consequently, alterations in the linker region could significantly impact P-gp's conformational transitions and its ability to transport substrates, making it also a potential target for therapeutic interventions aimed at modulating P-gp activity.

Modeling linker regions in ABC transporters presents challenges due to their large and flexible nature. These regions represent extensive domains, requiring careful consideration to avoid modeling artifacts. Incorporating the linker in our simulations provided new potential insights into its role in P-gp dynamics. Previous studies have suggested potential linker positions between both P-gp halves (between the NBDs) in an IF-open state [80]. However, for the OF conformation, the linker must be displaced from this position, indicating that its dynamics require further exploration during P-gp transitions. Our simulations revealed that the linker influences P-gp's dynamics and interactions with its environment. Specifically, we observed cholesterol penetration through the TM4-TM6 portal only when the linker was present, suggesting a potential entry route for other P-gp substrates with similar structures. This aligns with studies suggesting P-gp's role in membrane cholesterol redistribution [82]. Additionally, our simulations showed that the linker modulates the interactions between the ICLs and NBDs, affecting P-gp stability and function. Further exploration is needed to better understand its dynamics and the impact of phosphorylations in P-gp's regulation mechanisms.

## 5. Conclusions

In this study, we employed MD simulations to investigate the conformational dynamics of P-gp across its IF-open, IF-occluded, and OF states. By utilizing models derived from both the cryo-EM structures and AlphaFold database, we specifically examined the structural behaviors and functional implications of these conformational states, with an emphasis on the intricate role of the linker in P-gp functions. The conformational changes in P-gp, observed during its transitions between different states, resulted from the kinking and straightening of its TM helices. In the IF-occluded and OF conformations, overall lower correlations were found, indicating a weaker communication between the TMDs and the NBDs. We observed a more effective communication between the TMDs and NBDs in the IF-open state, which may be crucial to trigger conformational changes after the binding of a ligand. Our analysis was further enriched by the consideration of P-gp in complex with a chemotherapeutic substrate (VIN), and a third-generation inhibitor (ENC), allowing us to assess substrate translocation processes and inhibition mechanisms.

The insights gained from both ketMD and ABMD simulations provided a deeper understanding of the molecular mechanisms governing the functional cycle of P-gp. The application of ABMD simulations has been instrumental in shedding light on the role that local dynamics play in the transitions between distinct conformational states. The comparative analyses of the IF-open and -occluded conformations reveal distinct structural dynamics and functional implications for substrates and inhibitors. Notably, our simulations of the IF-occluded state highlighted a significant alteration at the interface between the TMDs and NBD2, suggesting a potential mechanism for the inhibition of P-gp.

A key finding of our study was the identification of specific amino acids and interactions serving distinct functions: some are crucial for conformational changes (e.g. F239 in TM4), while others are involved in attracting ligands (e.g. W232 in TM4). In particular, we demonstrated the multifaceted role of W232, not only in the conformational and functional cycle of P-gp but also in attracting various compounds, such as drugs or lipids, from the membrane.

Our study highlighted the challenges associated with achieving conformational transitions between the different P-gp states in the presence of the linker, addressing the complexities of its repositioning throughout these transitions. Interestingly, in systems including the linker, the observation of cholesterol penetration into the binding cavity highlighted a possible entry pathway for ligands, underlining the critical role of the TM4-TM6 portal in P-gp functions. The interaction between P-gp and membrane cholesterol provides a novel perspective on the transporter's broader role in cellular lipid regulation, with potential implications for targeting P-gp in conditions associated with cholesterol mismanagement.

Our findings have significant implications for understanding the molecular mechanisms of P-gp-mediated drug resistance. By elucidating the role of specific amino acids and structural conformations during P-gp activity, our study opens avenues for the design of new inhibitors that could modulate P-gp function and overcome multidrug resistance, a major challenge in cancer therapy.

## CRediT authorship contribution statement

**Balint Dudas:** Writing – review & editing, Methodology, Investigation, Formal analysis. **Salvatore Cisternino:** Writing – review & editing, Investigation, Formal analysis. **Xavier Declèves:** Writing – review & editing, Investigation, Funding acquisition, Formal analysis. **Maria A. Miteva:** Writing – review & editing, Supervision, Project administration,

Methodology, Investigation, Funding acquisition, Conceptualization. **Ahmad Elbahnsi:** Writing – review & editing, Writing – original draft, Visualization, Resources, Methodology, Investigation, Formal analysis, Conceptualization.

## Declaration of Competing Interest

The authors declare no conflict of interest.

## Acknowledgments

This work was supported by the French National Research Agency (project MetABC), Université Paris Cité and Inserm institute. Simulations were performed using High-Performance Computing (HPC) resources from Grand Equipement National de Calcul Intensif (GENCI)/ Centre Informatique National de l'Enseignement Supérieur (CINES) (Grant 2023-A0150314556, Adastra MI250 machine). The authors thank Dr. Isabelle Callebaut and Dr. Jean-Paul Mornon for insightful discussions.

### *Author contributions*

AE and MAM conceptualized the study. Funding was acquired by MAM and XD. Data collection, material preparations and simulations were performed by AE. Investigation and analyses were performed by all authors. The first draft of the manuscript was written by AE and all authors reviewed and edited the manuscript. All authors read and approved the final manuscript.

## Appendix A. Supporting information

Supplementary data associated with this article can be found in the online version at doi:10.1016/j.csbj.2024.06.010.

## References

[1] Thomas C, Tampé R. Structural and mechanistic principles of ABC transporters. Annu Rev Biochem 2020;89:605–36.
[2] Higgins CF. ABC transporters: from microorganisms to man. Annu Rev Cell Biol 1992;8:67–113.
[3] Rees DC, Johnson E, Lewinson O. ABC transporters: the power to change. Nat Rev Mol Cell Biol 2009;10:218–27.
[4] Chapy H, et al. Blood–brain and retinal barriers show dissimilar ABC transporter impacts and concealed effect of P-glycoprotein on a novel verapamil influx carrier. Br J Pharmacol 2016;173:497–510.
[5] Lee S-C, Arya V, Yang X, Volpe DA, Zhang L. Evaluation of transporters in drug development: current status and contemporary issues. Adv Drug Deliv Rev 2017; 116:100–18.
[6] Ai N, Fan X, Ekins S. In silico methods for predicting drug–drug interactions with cytochrome P-450s, transporters and beyond. Adv Drug Deliv Rev 2015;86:46–60.
[7] Juliano RL, Ling V. A surface glycoprotein modulating drug permeability in Chinese hamster ovary cell mutants. Biochim Biophys Acta BBA - Biomembr 1976; 455:152–62.
[8] Cordon-Cardo C, et al. Multidrug-resistance gene (P-glycoprotein) is expressed by endothelial cells at blood-brain barrier sites. Proc Natl Acad Sci 1989;86:695–8.
[9] Szöllősi D, Rose-Sperling D, Hellmich UA, Stockner T. Comparison of mechanistic transport cycle models of ABC exporters. Biochim Biophys Acta BBA - Biomembr 2018;1860:818–32.
[10] Clouser AF, Atkins WM. Long range communication between the drug-binding sites and nucleotide binding domains of the efflux transporter ABCB1. Biochemistry 2022;61:730–40.
[11] Sharom FJ. ABC multidrug transporters: structure, function and role in chemoresistance. Pharmacogenomics 2008;9:105–27.
[12] Callaghan R, Luk F, Bebawy M. Inhibition of the multidrug resistance P-glycoprotein: time for a change of strategy? Drug Metab Dispos Biol Fate Chem 2014;42:623–31.
[13] Tsuruo T, Iida H, Tsukagoshi S, Sakurai Y. Increased accumulation of vincristine and adriamycin in drug-resistant P388 tumor cells following incubation with calcium antagonists and calmodulin inhibitors. Cancer Res 1982;42:4730–3.
[14] Cornwell MM, Pastan I, Gottesman MM. Certain calcium channel blockers bind specifically to multidrug-resistant human KB carcinoma membrane vesicles and inhibit drug binding to P-glycoprotein. J Biol Chem 1987;262:2166–70.
[15] Dalton WS, et al. Drug-resistance in multiple myeloma and non-Hodgkin's lymphoma: detection of P-glycoprotein and potential circumvention by addition of verapamil to chemotherapy. J Clin Oncol 1989;7:415–24.
[16] Palmeira A, Sousa E, Vasconcelos H, M, Pinto M, M. Three decades of P-gp inhibitors: skimming through several generations and scaffolds. Curr Med Chem 2012;19:1946–2025.
[17] Pajeva IK, Wiese M. Structure–activity relationships of tariquidar analogs as multidrug resistance modulators. AAPS J 2009;11:435.
[18] Fox E, Bates SE. Tariquidar (XR9576): a P-glycoprotein drug efflux pump inhibitor. Expert Rev Anticancer Ther 2007;7:447–59.
[19] Alam A, Locher KP. Structure and mechanism of human ABC transporters. Annu Rev Biophys 2023;52:275–300.
[20] Huang J, Ecker GF. A structure-based view on ABC-transporter linked to multidrug resistance. Molecules 2023;28:495.
[21] Nosol K, et al. Cryo-EM structures reveal distinct mechanisms of inhibition of the human multidrug transporter ABCB1. Proc Natl Acad Sci 2020;117:26245–53.
[22] Urgaonkar S, et al. Discovery and characterization of potent dual P-glycoprotein and CYP3A4 inhibitors: design, synthesis, Cryo-EM analysis, and biological evaluations. J Med Chem 2022;65:191–216.
[23] Alam A, Kowal J, Broude E, Roninson I, Locher KP. Structural insight into substrate and inhibitor discrimination by human P-glycoprotein. Science 2019;363:753–6.
[24] Kim Y, Chen J. Molecular structure of human P-glycoprotein in the ATP-bound, outward-facing conformation. Science 2018;359:915–9.
[25] Barbieri A, et al. Structure of ABCB1/P-glycoprotein in the presence of the CFTR potentiator ivacaftor. Membranes 2021;11:923.
[26] Li J, Jaimes KF, Aller SG. Refined structures of mouse P-glycoprotein. Protein Sci 2014;23:34–46.
[27] Martin C, et al. Communication between multiple drug binding sites on P-glycoprotein. Mol Pharmacol 2000;58:624–32.
[28] Ferreira RJ, Ferreira M-JU, Dos Santos DJVA. Molecular docking characterizes substrate-binding sites and efflux modulation mechanisms within P-glycoprotein. J Chem Inf Model 2013;53:1747–60.
[29] Levring J, et al. CFTR function, pathology and pharmacology at single-molecule resolution. Nature 2023;616:606–14.
[30] Fiedorczuk K, Chen J. Molecular structures reveal synergistic rescue of Δ508 CFTR by Trikafta modulators. Science 2022;378:284–90.
[31] Chambers TC, Pohl J, Glass DB, Kuo JF. Phosphorylation by protein kinase C and cyclic AMP-dependent protein kinase of synthetic peptides derived from the linker region of human P-glycoprotein. Biochem J 1994;299:309–15.
[32] Szabó K, et al. Phosphorylation site mutations in the human multidrug transporter modulate its drug-stimulated ATPase activity. J Biol Chem 1997;272:23165–71.
[33] Esser L, et al. Structures of the multidrug transporter P-glycoprotein reveal asymmetric ATP binding and the mechanism of polyspecificity. J Biol Chem 2017; 292:446–61.
[34] Fiser A, Šali A. Modeller: Generation and Refinement of Homology-based Protein Structure Models. Methods in Enzymology, vol. 374. Elsevier; 2003. p. 461–91.
[35] Pettersen EF, et al. UCSF Chimera—a visualization system for exploratory research and analysis. J Comput Chem 2004;25:1605–12.
[36] Jumper J, et al. Highly accurate protein structure prediction with AlphaFold. Nature 2021;596:583–9.
[37] Varadi M, et al. AlphaFold protein structure database: massively expanding the structural coverage of protein-sequence space with high-accuracy models. Nucleic Acids Res 2022;50:D439–44.
[38] Roy A, Kucukural A, Zhang Y. I-TASSER: a unified platform for automated protein structure and function prediction. Nat Protoc 2010;5:725–38.
[39] Yang J, et al. The I-TASSER Suite: protein structure and function prediction. Nat Methods 2015;12:7–8.
[40] Vanommeslaeghe K, et al. CHARMM general force field: a force field for drug-like molecules compatible with the CHARMM all-atom additive biological force fields. J Comput Chem 2010;31:671–90.
[41] Jo S, Kim T, Iyer VG, Im W. CHARMM-GUI: a web-based graphical user interface for CHARMM. J Comput Chem 2008;29:1859–65.
[42] Lee J, et al. CHARMM-GUI input generator for NAMD, GROMACS, AMBER, OpenMM, and CHARMM/OpenMM simulations using the CHARMM36 additive force field. J Chem Theory Comput 2016;12:405–13.
[43] Kim S, et al. CHARMM-GUI ligand reader and modeler for CHARMM force field generation of small molecules: CHARMM-GUI ligand reader and modeler for CHARMM force field generation of small molecules. J Comput Chem 2017;38: 1879–86.
[44] Domicevica L, Koldsø H, Biggin PC. Multiscale molecular dynamics simulations of lipid interactions with P-glycoprotein in a complex membrane. J Mol Graph Model 2018;80:147–56.
[45] Lomize AL, Todd SC, Pogozheva ID. Spatial arrangement of proteins in planar and curved membranes by PPM 3.0. Protein Sci 2022;31:209–20.
[46] Lomize MA, Pogozheva ID, Joo H, Mosberg HI, Lomize AL. OPM database and PPM web server: resources for positioning of proteins in membranes. Nucleic Acids Res 2012;40:D370–6.
[47] Huang J, MacKerell AD. CHARMM36 all-atom additive protein force field: Validation based on comparison to NMR data. J Comput Chem 2013;34:2135–45.
[48] Klauda JB, et al. Update of the CHARMM all-atom additive force field for lipids: validation on six lipid types. J Phys Chem B 2010;114:7830–43.
[49] Abraham MJ, et al. GROMACS: High performance molecular simulations through multi-level parallelism from laptops to supercomputers. SoftwareX 2015;1–2: 19–25.
[50] Lindahl, Abraham, Hess & Van Der Spoel. GROMACS 2021.2 Manual. (2021) doi: 10.5281/ZENODO.4723561.
[51] Nosé S. A unified formulation of the constant temperature molecular dynamics methods. J Chem Phys 1984;81:511–9.

[52] Parrinello M, Rahman A. Polymorphic transitions in single crystals: a new molecular dynamics method. J Appl Phys 1981;52:7182–90.
[53] Darden T, York D, Pedersen L. Particle mesh Ewald: an *N* ·log( *N*) method for Ewald sums in large systems. J Chem Phys 1993;98:10089–92.
[54] Hess B, Bekker H, Berendsen HJC, Fraaije JGEM. LINCS: a linear constraint solver for molecular simulations. J Comput Chem 1997;18:1463–72.
[55] Dudas B, Decleves X, Cisternino S, Perahia D, Miteva MA. ABCG2/BCRP transport mechanism revealed through kinetically excited targeted molecular dynamics simulations. Comput Struct Biotechnol J 2022;20:4195–205.
[56] Marchi M, Ballone P. Adiabatic bias molecular dynamics: a method to navigate the conformational space of complex molecular systems. J Chem Phys 1999;110:3697–702.
[57] Tribello GA, Bonomi M, Branduardi D, Camilloni C, Bussi G. PLUMED 2: New feathers for an old bird. Comput Phys Commun 2014;185:604–13.
[58] Roe DR, Cheatham TE. PTRAJ and CPPTRAJ: software for processing and analysis of molecular dynamics trajectory data. J Chem Theory Comput 2013;9:3084–95.
[59] Kabsch W, Sander C. Dictionary of protein secondary structure: Pattern recognition of hydrogen-bonded and geometrical features. Biopolymers 1983;22:2577–637.
[60] Esque J, Oguey C, De Brevern AG. A novel evaluation of residue and protein volumes by means of laguerre tessellation. J Chem Inf Model 2010;50:947–60.
[61] Skjærven L, Yao X-Q, Scarabelli G, Grant BJ. Integrating protein structural dynamics and evolutionary analysis with Bio3D. BMC Bioinforma 2014;15:399.
[62] Westerlund AM, Fleetwood O, Pérez-Conesa S, Delemotte L. Network analysis reveals how lipids and other cofactors influence membrane protein allostery. J Chem Phys 2020;153:141103.
[63] Kang PW, et al. Calmodulin acts as a state-dependent switch to control a cardiac potassium channel opening. eabd6798 Sci Adv 2020;6. eabd6798.
64 Humphrey W, Dalke A, Schulten K. VMD: Visual molecular dynamics. J Mol Graph 1996;14:33–8.
[65] The PyMOL Molecular Graphics System, Version 2.0 Schrödinger, LLC.
[66] Nosol K, et al. Structures of ABCB4 provide insight into phosphatidylcholine translocation. Proc Natl Acad Sci 2021;118:e2106702118.
[67] Aller SG, et al. Structure of P-glycoprotein reveals a molecular basis for poly-specific drug binding. Science 2009;323:1718–22.
[68] Le CA, Harvey DS, Aller SG. Structural definition of polyspecific compensatory ligand recognition by P-glycoprotein. IUCrJ 2020;7:663–72.
[69] Barreto-Ojeda E, Corradi V, Gu R-X, Tieleman DP. Coarse-grained molecular dynamics simulations reveal lipid access pathways in P-glycoprotein. J Gen Physiol 2018;150:417–29.
[70] Fleetwood O, Kasimova MA, Westerlund AM, Delemotte L. Molecular insights from conformational ensembles via machine learning. Biophys J 2020;118:765–80.
[71] Liu Z, et al. Identification of binding sites in the nucleotide-binding domain of P-glycoprotein for a potent and nontoxic modulator, the amine-containing monomeric flavonoid **FM04**. J Med Chem 2023;66:6160–83.
[72] Bonito CA, et al. Probing the allosteric modulation of P-glycoprotein: a medicinal chemistry approach toward the identification of noncompetitive P-Gp inhibitors. ACS Omega 2023;8:11281–7.
[73] Loo TW, Clarke DM. Cysteines introduced into extracellular loops 1 and 4 of human P-glycoprotein that are close only in the open conformation spontaneously form a disulfide bond that inhibits drug efflux and ATPase activity. J Biol Chem 2014;289:24749–58.
[74] Klepsch F, Chiba P, Ecker GF. Exhaustive sampling of docking poses reveals binding hypotheses for propafenone type inhibitors of P-glycoprotein. PLoS Comput Biol 2011;7:e1002036.
[75] Mora Lagares L, et al. Homology modeling of the human P-glycoprotein (ABCB1) and insights into ligand binding through molecular docking studies. Int J Mol Sci 2020;21:4058.
[76] Verhalen B, et al. Energy transduction and alternating access of the mammalian ABC transporter P-glycoprotein. Nature 2017;543:738–41.
[77] Zhang Y, Gong W, Wang Y, Liu Y, Li C. Exploring movement and energy in human P-glycoprotein conformational rearrangement. J Biomol Struct Dyn 2019;37:1104–19.
[78] Behmard E, et al. Efflux dynamics of the antiseizure drug, levetiracetam, through the P-glycoprotein channel revealed by advanced comparative molecular simulations. Sci Rep 2022;12:13674.
[79] Ferreira RJ, Ferreira M-JU, Dos Santos DJVA. Insights on P-glycoprotein's efflux mechanism obtained by molecular dynamics simulations. J Chem Theory Comput 2012;8:1853–64.
[80] Ferreira RJ, Ferreira MU, Dos Santos DJVA. Assessing the stabilization of P-glycoprotein's nucleotide-binding domains by the linker, using molecular dynamics. Mol Inform 2013;32:529–40.
[81] Fiedorczuk K, Chen J. Mechanism of CFTR correction by type I folding correctors. Cell 2022;185:158–168.e11.
[82] Garrigues A, Escargueil AE, Orlowski S. The multidrug transporter, P-glycoprotein, actively mediates cholesterol redistribution in the cell membrane. Proc Natl Acad Sci 2002;99:10347–52.
[83] Szewczyk P, et al. Snapshots of ligand entry, malleable binding and induced helical movement in P-glycoprotein. Acta Crystallogr D Biol Crystallogr 2015;71:732–41.
[84] Mora Lagares L, Pérez-Castillo Y, Minovski N, Novič M. Structure–function relationships in the human P-glycoprotein (ABCB1): insights from molecular dynamics simulations. Int J Mol Sci 2021;23:362.
[8]5 Xing J, Huang S, Heng Y, Mei H, Pan X. Computational insights into allosteric conformational modulation of P-glycoprotein by substrate and inhibitor binding. Molecules 2020;25:6006.
[86] Rani P, Mandal P, Rajak BK, Singh DV. A review on dynamics of permeability-glycoprotein in efflux of chemotherapeutic drugs. Front Drug Discov 2024;4:1363364.
[87] Siarheyeva A, Liu R, Sharom FJ. Characterization of an asymmetric occluded state of P-glycoprotein with two bound nucleotides. J Biol Chem 2010;285:7575–86.
[88] Mora Lagares L, Pérez-Castillo Y, Novič M. Exploring the dynamics of the ABCB1 membrane transporter P-glycoprotein in the presence of ATP and active/non-active compounds through molecular dynamics simulations. Toxicology 2024;502:153732.
[89] Loo TW, Clarke DM. Locking intracellular helices 2 and 3 together inactivates human P-glycoprotein. J Biol Chem 2014;289:229–36.
[90] Loo TW, Clarke DM. Defining the drug-binding site in the human multidrug resistance P-glycoprotein using a methanethiosulfonate analog of Verapamil, MTS-verapamil. J Biol Chem 2001;276:14972–9.
[91] Morsy MA, et al. Carnosine potentiates doxorubicin-induced cytotoxicity in resistant NCI/ADR-RES Cells by inhibiting P-glycoprotein—in silico and in vitro evidence. Molecules 2022;27:7383.
[92] Chufan EE, et al. Multiple transport-active binding sites are available for a single substrate on human P-glycoprotein (ABCB1). PLoS ONE 2013;8:e82463.
[93] Ford RC, Marshall-Sabey D, Schuetz J. Linker domains: why ABC transporters 'live in fragments no longer'. Trends Biochem Sci 2020;45:137–48.